



Geologic CO₂ Sequestration Project Results

Introduction to Geologic CO ₂ Sequestration	2
Assessing Seal Capacity of Exploited Oil and Gas Reservoirs, Aquifers, and Coal Beds for Potential Use in CO ₂ Sequestration	7
Rapid Prediction of CO ₂ Movement in Aquifers, Coal Beds, and Oil and Gas Reservoirs	18
Geophysical Monitoring of Geologic Sequestration	51

For complete Technical Report, access: <http://gcep.stanford.edu/>

II.3 Introduction to Geologic CO₂ Sequestration

Fossil fuels currently dominate commercially supplied energy worldwide, and most estimates of energy use over the next 30 years suggest that use of fossil fuels will grow as the developing economies make greater use of energy. If that prediction is correct, then reduction of the amount of CO₂ emitted to the atmosphere will require that the CO₂ that results from combustion reactions be captured and stored. While many techniques are available for CO₂ separation, the cost of separation is still unacceptably high, and hence there is an opportunity for research in this area to lay the fundamental basis for more efficient separation methods. If the costs of separation can be reduced, then there is still the issue of where the CO₂ will be stored. This report deals with the possibility of storage in three geologic settings: oil and gas reservoirs, deep saline aquifers, and coalbeds. In each of these settings, sites will have to be selected that have appropriate geologic seals, efficient methods for flow predictions will be needed for process design and for permitting, and monitoring systems appropriate to various stages of a project will have to be designed. This report describes research to develop a suite of prediction tools appropriate to the flow settings and physical mechanisms that act and interact in the three geologic settings.

Oil reservoirs have considerable appeal as storage locations because they are known to have a geologic seal that trapped the hydrocarbons. Thus, as long as operations during oil production have not damaged that seal, the reservoir should be able to hold injected CO₂ indefinitely. Because oil (and also gas) reservoirs have known seals and because there is a regulatory structure that has experience in permitting gas-injection operations, existing oil fields are likely to be the first places that CO₂ sequestration is undertaken if it is to be done at large scale.

Storage of CO₂ can take place in zones in which CO₂ replaces reservoir oil or water. CO₂ is soluble in water, and it is about ten times more soluble in undisplaced oil. A separate CO₂-rich phase can also occupy significant pore volume. Movement of oil and gas in a reservoir is dominated by the pressure gradient created between injection and production wells and by the heterogeneity of the rocks. The viscosity of CO₂, a few hundredths of a centipoise over a wide range of pressures and typical reservoir temperatures, is low compared to most oils and any water present in the reservoir. The injected CO₂ invades high permeability flow paths as it makes its way to production wells. Accurate prediction of the timing of breakthrough of injected CO₂ at production wells and the amount of CO₂ produced with the oil requires detailed description of the permeability distribution in the reservoir. Those predictions are important because they forecast the amount of subsequent production, recompression, and recycling of CO₂ that is produced with oil.

CO₂ injection into gas reservoirs has been proposed but not yet been attempted. CO₂ could be used for pressure maintenance or for condensate vaporization, but the cost of purchasing CO₂ has so far prevented these applications in the absence of incentives for CO₂ storage. In fields that contain some condensate saturation, CO₂ can vaporize the light hydrocarbons that make up the condensate quite efficiently (see below), and it is even possible for CO₂ to develop multicontact miscibility with two-phase gas and condensate mixtures¹. If CO₂ sequestration were undertaken in a substantial way, gas reservoirs would be candidate storage locations, again with a known geologic seal capable of holding gas indefinitely.

Storage of CO₂ in a gas reservoir would have the advantage that all CO₂ that results from oxidation of CH₄ produced from the reservoir could be stored in the same reservoir, at the same temperature and pressure, with volume left over. One mole of CO₂ is produced for each mole of CH₄ oxidized, and the molar density of CO₂ is always larger than that of CH₄ at a given temperature and pressure. Figure 1 shows molar densities of CH₄ and CO₂ calculated with the Peng-Robinson equation of state² with volume translation³. The higher molar density of CO₂ means that the volume of CH₄ produced from a gas reservoir could be replaced by a mixture of N₂ and CO₂. In other words separation of all of the N₂ from a flue gas, for example, would not be required to match injection and withdrawal volumes, although there would be additional cost associated with compression of the N₂/CO₂ mixture over that for CO₂ alone. Figure 2 shows that a mixture of 60% N₂ and 40% CO₂ has approximately the same density as pure CH₄ at 50, 75, and 100C.

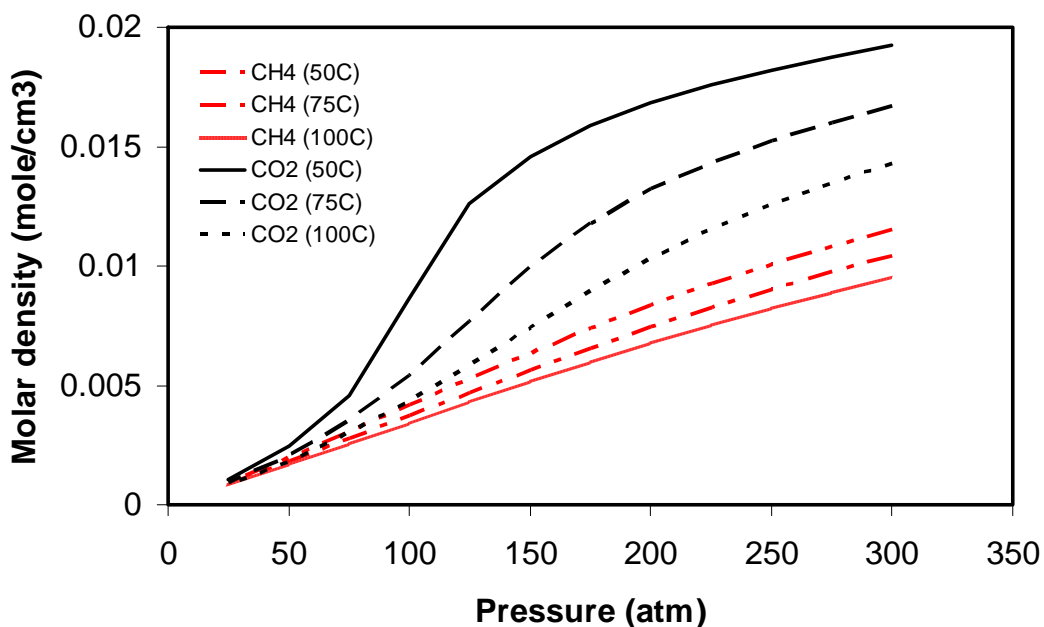


Figure 1: Molar density of CH₄ and CO₂.

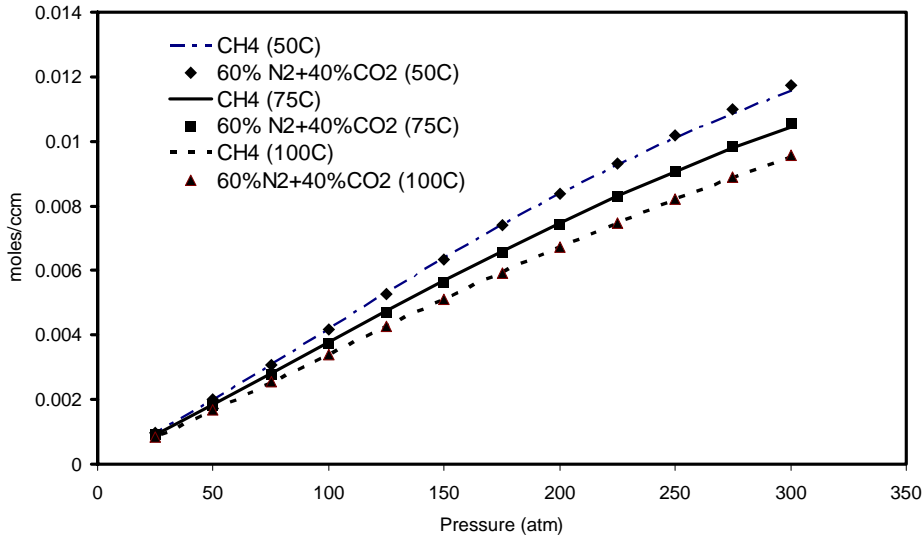


Figure 2: Molar density of CH₄ and a mixture containing 60% N₂ and 40% CO₂.

Oil and gas reservoirs are not uniformly distributed geographically, and there are many locations where anthropogenic CO₂ is generated that are not close to potential storage sites in oil or gas reservoirs. Deep formations that contain salt water are more widely distributed, however.

In this setting, injected CO₂ will also flow more easily through high permeability paths, but the flow will not be dominated by the pressure gradients imposed by injection and production wells. Gravity segregation caused by the difference in density of the injected CO₂ and brine will cause preferential flow at the top of the aquifer, though injection of the CO₂ well below the top of the aquifer can mitigate this gravity segregation to some extent. Aquifers with large volume, reasonable permeability and thickness, and good pressure communication over long distances will be most attractive, so that large volumes could be injected without raising aquifer pressure significantly. The injected CO₂ will dissolve, eventually, in the brine, and the resulting brine/CO₂ mixture will be slightly denser than the brine alone^{4,5}. Slow vertical flow of the denser brine will cause further dissolution, as fresh brine is brought in contact with the CO₂ phase. Trapping of a separate CO₂ phase by brine can also act to immobilize CO₂ as a residual phase⁵. Estimates of the time scales for dissolution and the resulting vertical convection suggest that hundreds to thousands of years will be required to dissolve all the CO₂^{4,5}, but by that time, much of the CO₂ will exist in a trapped residual phase⁵. Relatively slow chemical reactions, depending on the chemical composition of the brine and the minerals present in the aquifer may then sequester some of the CO₂ as minerals⁶.

In oil and gas reservoirs and aquifers, injected CO₂ occupies the pore space as a separate phase or is dissolved in water or oil. Deep, unmineable coal beds offer a different storage mechanism—the same mechanism that is the source of coal bed methane. Gases like CH₄ or CO₂ adsorb at high pressure on the surfaces of coal particles. They show what is typically observed: significantly more CO₂ adsorbs at a given

pressure and temperature on coal than does CH₄ or N₂. In addition, the hysteresis of the adsorption curves suggests that once the CO₂ is adsorbed, much of it will stay adsorbed even if the pressure is decreased at a later time.

Flow in coal beds will occur primarily in the fracture network (fractures in coal are known as cleats). Injected CO₂ will flow through the cleats, diffusing into matrix blocks, where replacements of adsorbed CH₄ by CO₂ will occur⁷. If that replacement occurs at reasonable rates, CO₂ can be used to enhance CH₄ recovery. This displacement process is similar to adsorption chromatography. Because CO₂ adsorbs more strongly than either CH₄ or N₂, it should be possible to use the coal bed to separate a mixture of N₂ and CO₂⁸, though at the cost of compression of the N₂ in addition to the CO₂ and the separation of N₂ from produced CH₄. There is evidence that coal permeability changes with the amount of adsorbed gas. As CH₄ is removed from coal, permeability typically increases, and as CO₂ adsorbs, permeability decreases. Thus, displacement processes in coal beds will involve a complex interplay of flow in the cleat system, changes in permeability, diffusion, and adsorption.

An important question, of course, is whether there is sufficient capacity available for storage of large quantities of CO₂ in the subsurface. Table I summarizes two sets of estimates of storage capacity in the subsurface. The ranges of the numbers are very large, an indication of the uncertainty in the estimates. Even so, the estimates are large enough to suggest that there is sufficient capacity to store a significant fraction of expected CO₂ emissions through 2030 and beyond. Current emissions are about 24 GtCO₂/yr (1 GtCO₂ = 1 billion metric tons of CO₂), and according to the estimates of the International Energy Agency¹⁰, are expected to rise to 38 GtCO₂/yr. If the rise in emission were roughly linear, then the total emissions would be about 1300 GtCO₂ for the period from 2000 to 2030. Thus, even given the uncertainty in the estimates, the capacity of geologic formations to store CO₂ appears to be sufficient to permit storage at significant scale.

Table I: Estimated storage capacities of geologic formations (GtCO₂).

Storage Option	Parson & Keith ⁹	Gale ¹⁰
Oil and gas reservoirs	740-1850	920
Deep saline aquifers	370-3700	400-10,000
Coal beds	370-1100	40

The existence of volumetric storage capacity is not sufficient, of course, to guarantee that CO₂ injection into the subsurface can be undertaken at scale. Many individual projects would be needed to accommodate the volumes of CO₂ that would have to be injected. For example, the Sleipner Project¹² is currently injecting about 10⁶ tCO₂/yr into a high permeability sandstone formation in the North Sea. One thousand similar projects would be required to store 1 GtCO₂/yr, and if the injected CO₂ had a density of 500 kg/m³ at reservoir conditions, the total injected volume would be about 34 million barrels per day. Thus, handling even 1 GtCO₂/yr, about 4% of current emissions, would require

substantial investment in separation capacity, infrastructure for transportation of the CO₂, and wells and facilities for injection.

Identification of appropriate sites for geologic storage of CO₂ will require work to establish that the injected CO₂ will be retained in the subsurface. Research on the filling of oil and gas reservoirs indicates that stress changes associated with injection or depletion can affect the integrity of the geologic seals that contain the fluids^{13,14}. Accumulation of oil, gas, or CO₂ can activate faults and cause leakage or can change the state of stress in such a way that leakage is less likely, so careful analysis will be required. More is likely to be known about the state of stress in oil and gas reservoirs than for aquifers or coal beds, so there will be a need for additional research in this area. Wellbores, which always penetrate the geologic seal, offer one potential pathway for leakage. Care will have to be taken to avoid sites and formations where there are abandoned wells that offer leak paths, and active wells will need to be well maintained. While operations at significant scale in enhanced oil recovery projects indicate that it is possible to conduct CO₂ injection safely, careful attention will be needed to maintain safe operations in the many injection projects that will be required if geologic storage of CO₂ is to take place at large scale.

Appropriate levels of monitoring of storage projects will also be needed. It is likely that more monitoring will be needed early in the life of a project than will be required later, but appropriate methods will need to be established for the various stages of a project. A variety of monitoring techniques have potential for use in CO₂ storage projects. Seismic methods, which include time-lapse reflection¹⁵ or tomographic imaging¹⁶ and possibly passive seismic approaches can be used to detect subsurface migration and leaks. Gravity measurements and deformation methods such as synthetic aperture radar or tiltmeter measurements also have potential, though they will provide lower resolution indications of fluid movement.

Finally, use of geologic storage of CO₂ at large scale will require establishing appropriate permitting processes¹⁷ for projects in deep saline aquifers, and perhaps for coal beds in some locations. It will be important in the design and permitting of projects to choose sites where the geologic seals provide long-term containment, to predict where the injected CO₂ will migrate during injection, to monitor at appropriate levels where the injected CO₂ has gone, and to understand the ultimate fate of the injected CO₂. While a solid base of experience exists, there is much more to be done to design and optimize large-scale CO₂ storage projects in geologic formations. In the remainder of this report, we consider three areas of research related to geologic storage of CO₂: seal capacity, prediction of fluid movement, and monitoring.

II.3.1 Assessing Seal Capacity of Exploited Oil and Gas Reservoirs, Aquifers, and Coal Beds for Potential Use in CO₂ Sequestration

Investigators

M. D. Zoback, Professor of Geophysics; Amie Lucier, Lourdes Colmenares, Graduate Research Assistants

Background

In order for geologic CO₂ sequestration to be an effective tool in the stabilization of atmospheric CO₂ concentrations, a goal of sequestering about 3 Gt of carbon per year (~10 Gt CO₂/y) must be met by mid-century (based on current emissions predictions). Currently, pilot CO₂ sequestration projects such as Weyburn in Canada and Sleipner in the North Sea are sequestering on the order of 1 Mt CO₂/y. These pilot projects are important testing grounds for issues that will be faced as we move towards widespread sequestration implementation. It is important to look forward to the future of CO₂ sequestration and continue to evaluate the potential of as many large capacity repositories as possible.

Three options for geologic storage are unmineable coal seams, deep saline aquifers, and mature oil and gas fields. In the future, it will likely be necessary to exploit all of these possible options in order to make a significant impact on global atmospheric CO₂ concentrations. Coal seams offer the unique and attractive ability to store CO₂ by adsorbing it onto the coal surface. CO₂ injected for sequestration purposes can also be used to enhance the production of coal bed methane (CBM). Deep saline aquifers may provide the most capacity of the three storage options, but most are often poorly characterized as to their structure and physical properties. They are important sites because deep saline aquifers can be found in most areas with large numbers of CO₂ point sources, such as coal-burning power plants. Depleted oil and gas fields offer attractive benefits such as partially in-place infrastructures, extensive databases, and the possibilities for value-added benefits from enhanced oil recovery (EOR) and possibly enhanced gas recovery (EGR). Oil and gas fields have also contained large volumes of buoyant fluids for geologic periods of time, which means that at least in the past they had adequate seal integrity. The fact that hydrocarbon production is occurring suggests that the reservoir has a certain level of porosity and permeability as well as a reasonable capacity, which indicates that injection of CO₂ into the reservoir would be possible.

We are engaged in three parallel studies investigating geomechanics applied to seal integrity and CO₂ sequestration in geologic formations. These projects cover all three options for geologic CO₂ sequestration:

- Unmineable Coal Seams:
 - Powder River Basin (PRB)
 - Collaboration with Western Resources Project Foundation and Dr. Jonny Rutqvist at Lawrence Berkeley National Laboratory
- Deep Saline Aquifers:
 - Ohio River Valley CO₂ Storage Project

- Collaboration with Battelle, DOE, NETL, American Electric Power, BP, Schlumberger, Ohio Coal Development Office
- Depleted Oil & Gas Reservoirs:
 - Gulf of Mexico, South Eugene Island 330
 - Collaboration with ExxonMobil

CO₂ Sequestration and ECBM in Unmineable Coal Seams

Coal seams are both a source of methane and a carbon-dioxide sink. For sub bituminous coal like the ones in the Powder River Basin (Figure 3), the CO₂/CH₄ ratio is approximately 10:1 (Figure 4), which indicates the great potential of the Powder River Basin to sequester this greenhouse gas. In addition, CO₂ can also be used to enhance the production of CH₄ from the coal seam since CO₂ has higher adsorption capacity than CH₄ in coal (see Figure 3). This means that the injection of CO₂ in coal beds works for sequestering CO₂ and also enhanced coal bed methane production (ECBM).

From our previous work in the Powder River Basin, we have found that it is typical during drilling and completion operations for the “water-enhancement” activities in the coal seams to result in hydraulic fracturing of the coal and possibly the adjacent strata thereby resulting in both excess CBM water production and inefficient depressurization of coals. We have been able to collect water-enhancement test data in coals to obtain the magnitude of the least principal stress in the coal seam. The preliminary data we have analyzed indicates that the hydrofracs are horizontal in some areas, such that vertical fracture growth is not a problem. However, vertical fracture growth does appear to occur in some places in the Powder River Basin. We are investigating the idea of using the hydrofracs that have been produced in the coals as a more effective path to inject CO₂ for sequestration and ECBM.

CO₂ Sequestration in Deep Saline Aquifers

Several sequestration projects are looking at the deep saline aquifers in the Ohio River Valley as potential sites for CO₂ sequestration because of the large number of CO₂ point sources located in the Midwest. The Ohio River Valley CO₂ Storage Project is unique because it is a field investigation located on the site of the coal-burning Mountaineer Power Plant (Figure 5). Much of the field data needed to characterize the site has already been collected. A 2-D seismic survey through the site was collected in July of 2003. A 9190 ft well was drilled from May through July of 2003. The well was logged with a full suite of geophysical tools, including a Formation MicroImager (FMI) tool. Extensive core and brine sampling was also done. Pressure tests to determine the magnitude of the least principal stress are currently being performed in the well. All of this data is being analyzed to characterize the aquifer and the caprock for their CO₂ sequestration potential.

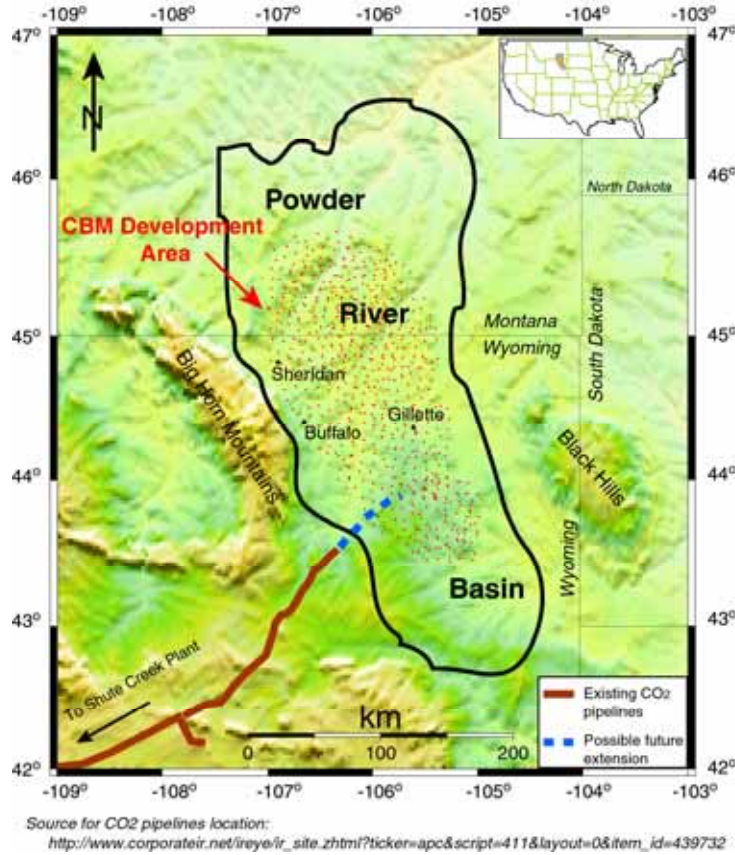


Figure 3: Topographic relief map of the Powder River Basin in Montana and Wyoming. The red dots cover the CBM development area. An existing CO₂ pipeline runs towards the southwest boundary of the basin, and there is a possibility that this could be extended into the PRB in the future.

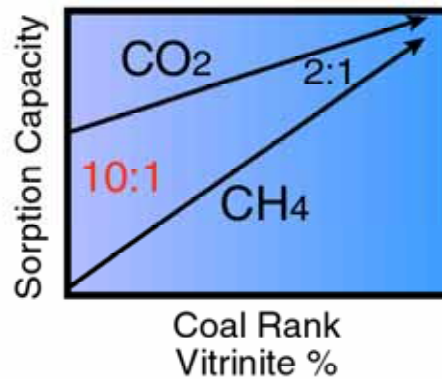


Figure 4: Sorption capacity with respect to Coal Rank. The replacement ratio of CO₂-to-CH₄ is highest for low rank coals, e.g. sub bituminous coals (Bustin *in* Reeves¹⁸, 2003). The coal found in the Powder River

Basin is sub bituminous, making it a great candidate for CO₂ sequestration.

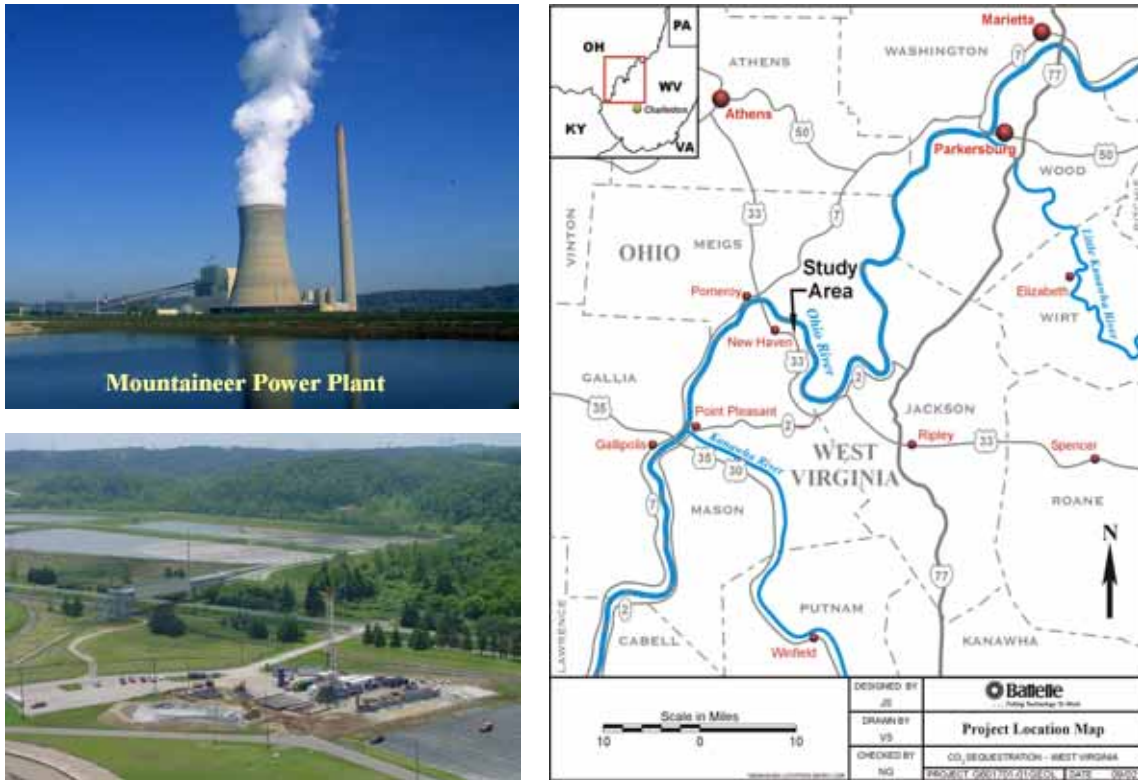


Figure 5: Location of the Mountaineer Power Plant, New Haven, WV. The pilot well (bottom left) for the Ohio River Valley CO₂ Storage Project was drilled on site at the power plant during the summer of 2003 (figures from Gupta¹⁹).

CO₂ Sequestration in Depleted Oil and Gas Fields

Depleted oil and gas fields seem to be the natural choice for the first large-scale CO₂ sequestration operations. Currently, one of the largest CO₂ sequestration projects in an oil and gas field is taking place in the Weyburn field in the Williston Basin of Saskatchewan, Canada. The project combines CO₂ sequestration with EOR operations to store about one million tons of CO₂ per year. This is an extremely small fraction of the amount of CO₂ that must be sequestered to make a significant impact on stabilizing atmospheric CO₂ concentrations.

We are beginning to examine the sequestration potential of fields in the Gulf of Mexico by developing a workflow for assessing reservoir suitability for sequestration. There are a number of factors that make the Gulf of Mexico an appropriate site for developing a regional workflow. Extensive datasets are available that are crucial in building a comprehensive picture of the potential storage sites. The current petroleum industry infrastructure and the number of CO₂ sources near the Gulf Coast are integral steppingstones in the building of a complete CO₂ sequestration infrastructure (Figure 6).

There is also significant capacity for storage in the region as well as potential for value-added benefits from CO₂ EOR.



Figure 6: Map of the U.S. Gulf Coast and Gulf of Mexico and some of the existing infrastructure in the region²⁰. Oil pipelines are in green, gas pipelines in red, and onshore pipelines in gray. The black figures are possible sources where anthropogenic CO₂ that could be captured and separated for sequestered in the Gulf of Mexico. In yellow is the location of our case study site, South Eugene Island Block 330.

Results

Powder River Basin

The first step in studying CO₂ sequestration coupled with ECBM in the unmineable coal seams of the Powder River Basin is mapping out areas where horizontal hydrofractures occur rather than vertical ones. Hydrofracs open horizontally when the least principal stress is the vertical stress (S_v). The magnitude of the least principal stress is determined by pressure tests like the water-enhancement tests. We can calculate S_v by integrating over the density log. If these two values are the same, horizontal hydrofracs can occur when the fluid pressures exceed the magnitude of the least principal stress.

Our next step is to run simulations of various injection scenarios. As shown in Figure 7, we intend to use stacked hydrofracs in the coal to inject CO₂ and produce CH₄. Specifically, we will investigate the efficiency of producing a hydrofrac towards the bottom of a coal seam where CO₂ would be injected, and a hydrofrac in the upper part of the coal seam from which CH₄ and water would be produced. The simulations have the following objectives:

- Examine multiphase flow characteristics of CO₂-H₂O-CH₄ system
- Test for hydrofrac spacing, thickness of coal seam, spacing of wells
- Investigate rates and volumes of sequestered CO₂ and produced CH₄

We also expect to find alternative ways of sequestering CO₂ in a specific setting like the PRB, which could take advantage of existing wells and hydrofracs during the injection of CO₂ into the coal.

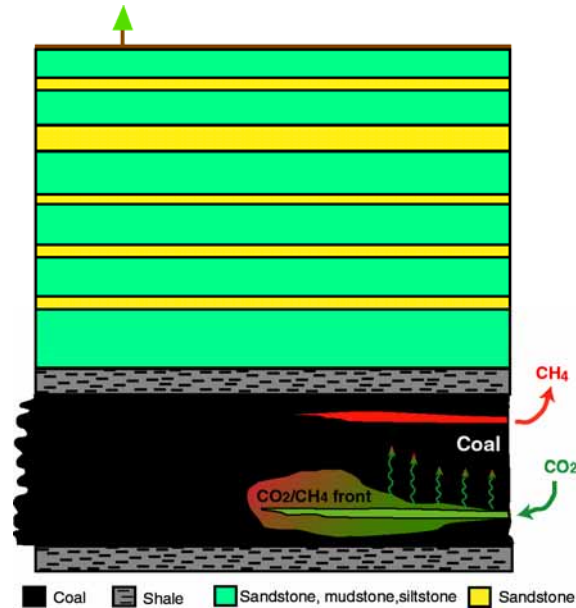


Figure 7: Schematic of suggested ECBM configuration. CO₂ is injected into the deeper horizontal hydrofrac. As the CO₂ front moves through the coal and is preferentially adsorbed, it displaces the methane. The free methane is then produced from a shallower horizontal hydrofrac.

1. To do these simulations, we have been collaborating with Dr. Jonny Rutqvist from the Lawrence Berkeley National Lab. The computer code we are using is TOUGH2 with the CBM module added to it. TOUGH2 is a numerical simulator for nonisothermal flows of multicomponent, multiphase fluids in one-, two-, and three-dimensional porous and fractured media (Pruess *et al.*²¹). Modifications were made to one of the original modules of TOUGH2 to be able to apply it to ECBM simulations (Webb²²). The extended Langmuir isotherm for sorbing gases, including the change in porosity associated with the sorbed gas mass, has been included in the new ECBM module. We have started to build our code by creating meshes that would represent the structure that we want to study (described above, Figure 7) and during the test simulations, we are feeding the code real data.

2.

Ohio River Valley CO₂ Storage Project

We are developing a comprehensive geomechanical model of the Ohio River Valley CO₂ Storage Project site. This is an integral step in the complete characterization of a potential CO₂ storage site that provides a good indication as to the suitability of these aquifers for long-term storage of anthropogenic CO₂. In particular, we are examining the

state of stress and fracture characteristics in the Rose Run aquifer as well as the layers adjacent to this formation. We have used the FMI log to pick the drilling-induced tensile fractures along the wellbore (Figure 8). These propagate in the direction of greatest horizontal stress, S_{Hmax} . The minimum horizontal stress, S_{Hmin} , is oriented 90° from S_{Hmax} . From the drilling-induced tensile fractures, we have determined that S_{Hmax} is oriented N47°E, and S_{Hmin} is oriented N43°W (Figure 8). This is consistent with the regional stress. The presence of en echelon tensile fractures in the near-vertical wellbore indicates localized stress perturbations exist (Figure 8). The next steps in this study are to compile a pore-pressure profile of the well, the results of ongoing mini-frac tests to determine the magnitude of S_{Hmin} , and to integrate over the density log to get the vertical stress. Using this information, we can constrain the magnitude of S_{Hmax} to complete our geomechanical model of the site. We have also used the FMI data to pick natural fractures that cross the wellbore.

We plan to use our geomechanical model and fracture characterization to determine the distribution and orientation of hydraulically conductive fractures within the aquifer and the effectiveness of adjacent layers to act as seals against the vertical migration of the injected CO₂. By assessing the magnitude of the least principal stress in the Rose Run aquifer, we will determine the injection pressure at which hydraulic fracturing will occur as well as the direction of the hydraulic fracture propagation. This is fundamental in the development of a safe and effective injection plan. We will also determine the maximum fluid pressures that can be maintained in the formations (i.e., their dynamic capacity) without resulting in frictional failure and leakage through hydraulically active fractures.

Gulf of Mexico

It is imperative to approach any assessment of CO₂ storage potential in the Gulf of Mexico from a geomechanical perspective. Many of the trapping mechanisms in the region depend on fault seal. So it is necessary to determine the initial state of the trapping and sealing mechanisms, examine the effect of production on the seal, and predict changes associated with CO₂ injection and storage (Figure 9). A complete geomechanical model is important in assessing the reservoir and seal conditions throughout the lifetime of the reservoir. We are using South Eugene Island Block 330 (SEI 330) as a case study site to develop and test a geomechanical workflow for assessing CO₂ sequestration potential in the Gulf of Mexico.

South Eugene Island Block 330 is located offshore of Louisiana about 270 km southwest of New Orleans. The field is part of a salt-withdrawal, plio-pleistocene mini-basin. Most of the reservoirs in the field are in the hanging wall of the major basin-bounding normal growth fault. Hydrocarbons are trapped by rollover anticlines created during salt-withdrawal related faulting. It is a mature field that was discovered in 1971 and began production in 1972. An extensive dataset exists for the field, including a recent 3D seismic survey, numerous well logs, bottom-hole pressure readings, and pressure tests (leak-off tests and formation integrity tests).

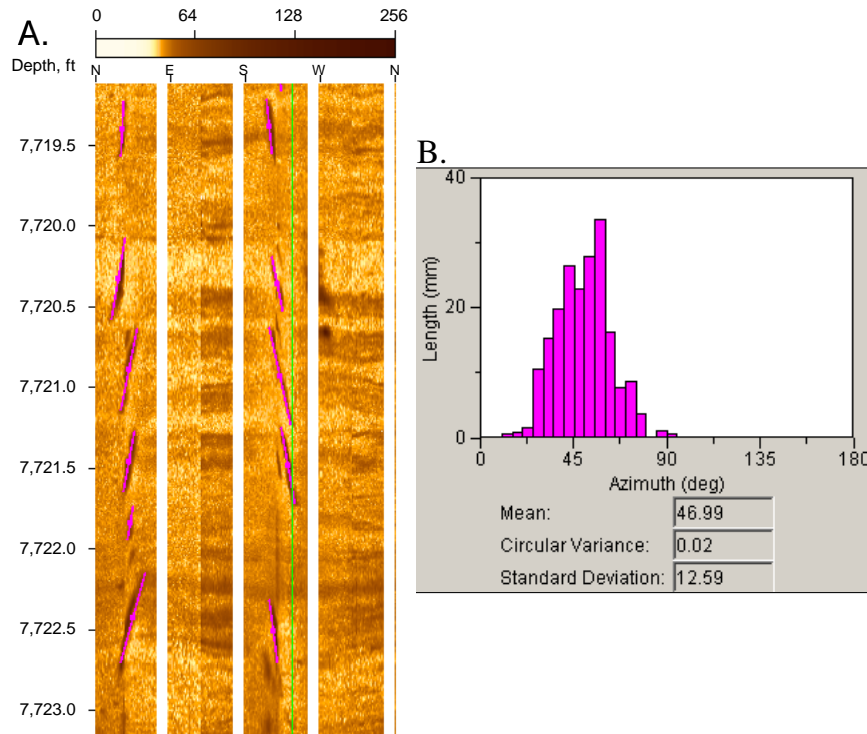


Figure 8: Drilling-induced tensile fractures from the AEP#1 well drilled on site at the Mountaineer Power Plant in New Haven, WV. A) FMI image showing an echelon drilling-induced tensile fractures. The color scale is conductivity. The green line shows the orientation of caliper 1; the pink lines are picks of the individual fractures. B) A plot of azimuth vs. length of the tensile fractures picked from 6400 ft to 9100 ft. The mean azimuth is 47°, so we estimate that the orientation of S_{Hmax} is N47°E.

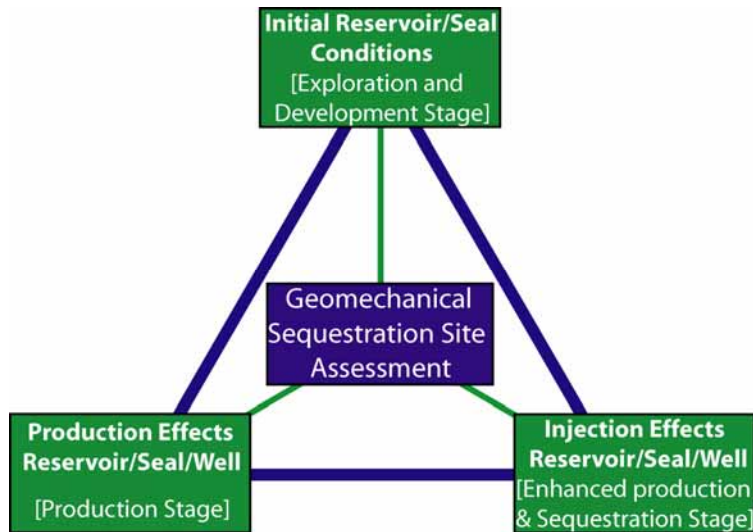


Figure 9: The strategy for building a geomechanical sequestration site assessment is to integrate data from the three stages in the lifetime of a field.

Dynamic constraints on hydrocarbon fill are of interest when looking at this field as a possible site for CO₂ sequestration. Dynamically controlled reservoirs are pressure-limited rather than volume-limited, making it more difficult to determine the capacity of the reservoir for CO₂ storage. Examples of dynamic controls on hydrocarbon fill are capillary entry pressure of the caprock, hydraulic fracture limit (equal to the magnitude of the least principal stress), and dynamic fault-slip limit (equal to a critical pore pressure based on the state of stress and Coulomb failure criterion). When any one of these pressure limits is reached at the top of a reservoir, the caprock cannot support any additional hydrocarbons. If additional hydrocarbons enter the system, the dynamic control acts to release the fluids, through capillary entry, hydraulic fracturing or dynamic fault slip, which decreases the buoyant pressure on the caprock (Figure 10). This presents a unique problem when injecting CO₂ into dynamically constrained reservoirs. Because the density of CO₂ at normal reservoir conditions is about 500-700 kg/m³ depending on temperature-and-pressure conditions, an oil reservoir can hold a smaller volume of CO₂ than oil, but a gas reservoir can support a larger volume of CO₂ than gas (Figure 10). In reality, the fluids in a reservoir undergoing sequestration operations will be a complex, time-dependent mixture of oil, gas, and CO₂. Therefore, it is important to fully understand the initial controls limiting hydrocarbons in the reservoir prior to production and have production history data to be able to estimate the capacity of reservoir to store CO₂.

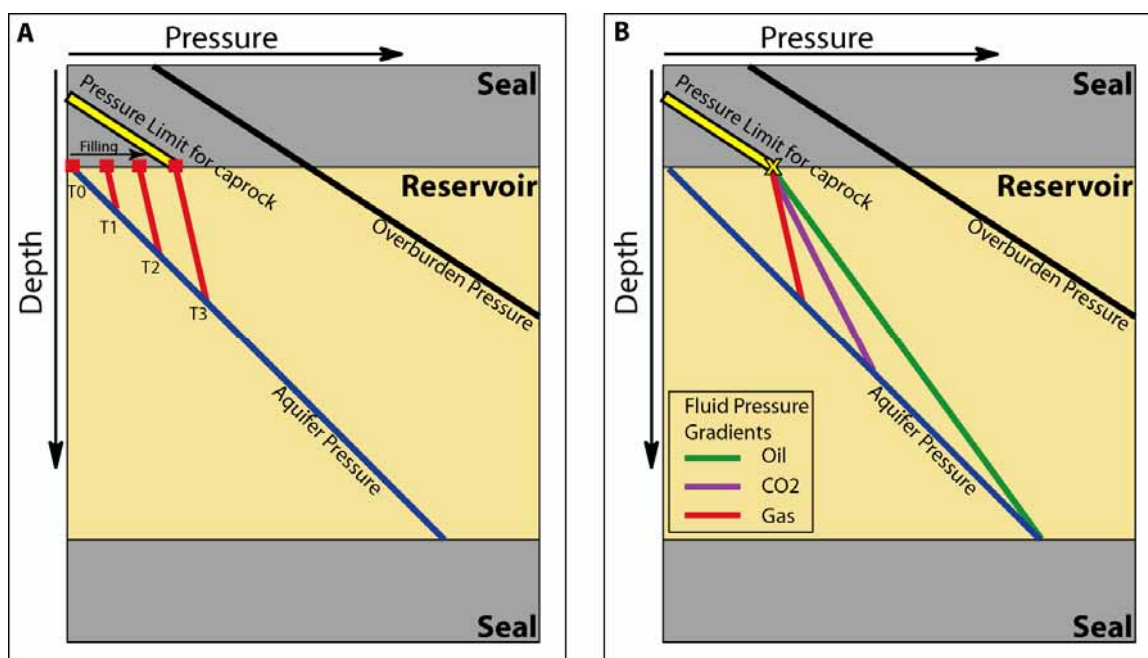


Figure 10: Effect of buoyant fluids on reservoir capacity in the presence of pressure-limited seals. A) Modified from Finkbeiner *et al.*²³, at T₀ there are no hydrocarbons in the reservoir, and the pressure at the cap rock falls along the pressure gradient of water in the aquifer. As the reservoir fills through time from T₀ to T₃, the pressure at the top of the reservoir increases, falling along the hydrocarbon pressure gradient. When the buoyancy force on the cap rock equals the pressure limit, the seal cannot support any additional

hydrocarbons. B) The different buoyancies of oil, CO₂, and gas affect the volumes of these fluids that can be sustained by a pressure-limited seals.

A study by Finkbeiner *et al.*²³ shows that dynamic controls on hydrocarbon fill exist in some of the reservoirs in South Eugene Island 330. One example of a dynamically controlled reservoir is the OI-1 sand in Fault Block A. Figure 10, which is modified from Finkbeiner *et al.*²³, is a pressure vs. depth plot that illustrates the dynamic fault-slip limit is acting as a control on the seal capacity of the OI-1 sand in Fault Block A. The blue line is hydrostatic pressure, and the black line is the overburden pressure. The green dashed line is the hydraulic fracture limit or least horizontal stress, interpolated from leak-off tests and formation integrity tests. The yellow box is the dynamic slip limit calculated from the overburden stress and the least horizontal stress over a range of coefficients of friction between 0.3 and 0.6. The oil columns are shown in green, and the gas columns in red. The pressure at the top of the oil leg reaches the dynamic fault slip limit, suggesting that this reservoir is controlled by dynamic fault slip. However, other shallower sands in the same fault block are clearly not limited by the dynamic fault slip or hydraulic fracture limit.

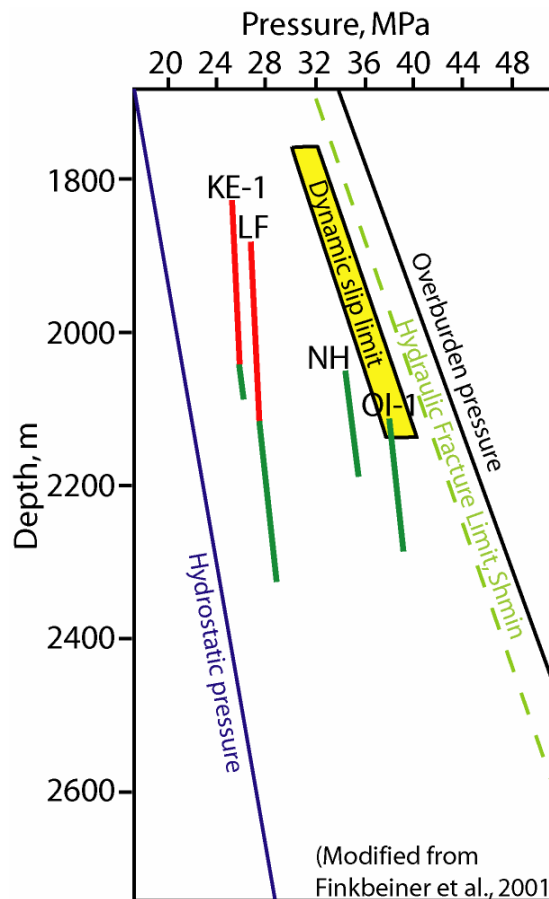


Figure 11: Pressure vs. depth plot of SEI 330 Fault Block A. The oil column in the OI-1 sand appears to be controlled by the dynamic slip limit, while the other shallower sands are not limited by that dynamic control. See text for more explanation. We are developing

a geomechanical workflow in the context of the SEI 330 field (Figure 12). We have chosen to study this field in more detail because previous studies have brought a number of interesting yet unresolved questions to light about topics such as the relationships between fault blocks, fluid migration, sources of overpressure and controls on hydrocarbon column heights (Alexander and Flemings²⁴; Alexander and Handschy²⁵; Gordon and Flemings²⁶; Losh *et al.*²⁷; Stump and Flemings²⁸; Finkbeiner *et al.*²³; Losh *et al.*²⁹, and others). Many of these studies are based on the structure maps generated by Pennzoil over a decade ago. Currently, ExxonMobil is creating structure maps based on a newer 3D survey using the advanced interpretation tools now available. We will reevaluate SEI 330 based on these new structural interpretations and see if this affects the interpretations that were made in the previous studies.

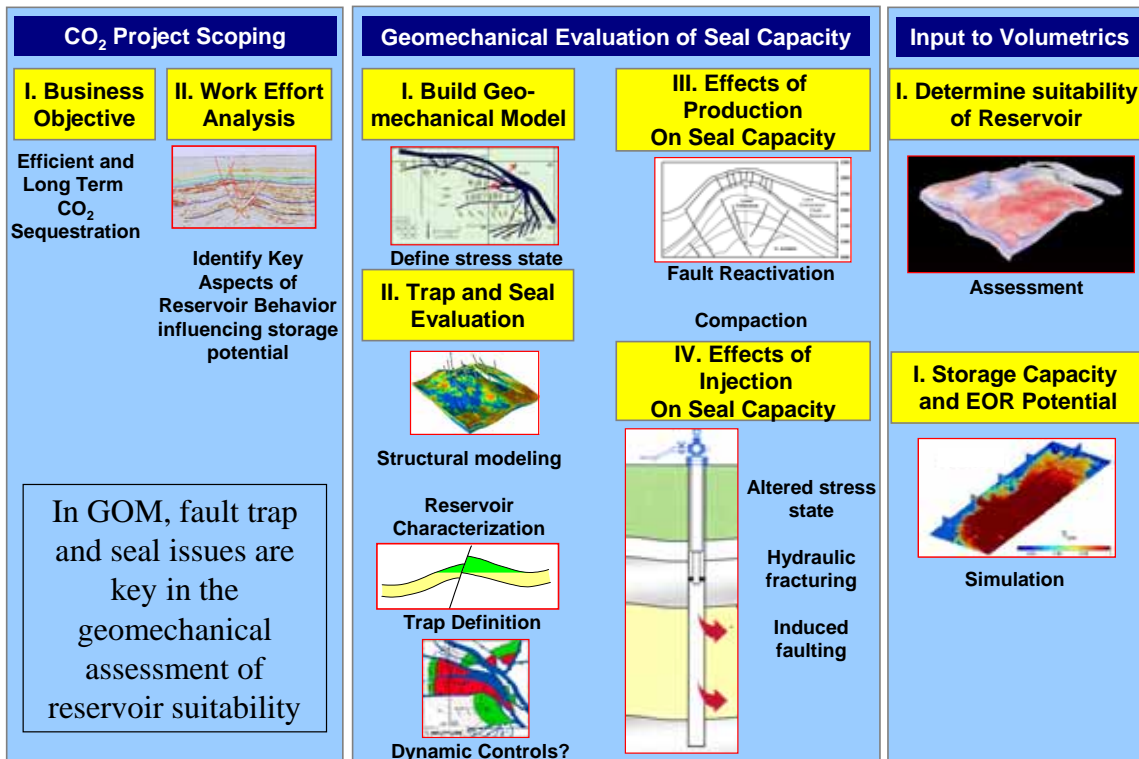


Figure 12: Initial draft of the Workflow for Assessing Reservoir Suitability for CO₂ Sequestration in the Gulf of Mexico.

II.3.2 Rapid Prediction of CO₂ Movement in Aquifers, Coal Beds, and Oil and Gas Reservoirs

Investigators

A. R. Kavscek, Associate Professor, Petroleum Engineering; F. M. Orr Jr, Professor, Petroleum Engineering Department; K. Jessen, Acting Assistant Professor, Petroleum Engineering Department, G. Q. Tang, Research Associate, M. D. Cakici, Marc Hesse, C. J. Seto, Graduate Research Assistants

Background

Considerable effort has been devoted to the development of reservoir simulation tools for the oil industry, and there are high-quality simulators available that handle effectively many of the flow problems appropriate to oil and gas reservoirs. One area where simulator development is continuing, however, is in the simulation of processes in which multiple components transfer between whatever phases are present in the porous medium. Injection of CO₂ into geologic reservoirs inevitably involves such component transfers, as the injected CO₂ dissolves in any water or oil present, as hydrocarbons transfer to the relatively dense CO₂-rich phase, or as CO₂, methane, and possibly N₂ adsorb and desorb in coal.

Because the most important physical mechanisms of storage differ for the three geologic systems, it is appropriate to consider the current state of predictive models for each setting. Compositional simulation tools are best developed for oil and gas reservoir settings, for which several fully capable finite-difference compositional simulators are available. ECLIPSE 300 and GEM are examples. These codes use an equation of state to represent equilibrium partitioning of components between oil and gas phases, and they handle the effects of capillary pressure and gravity well. The principle limitations of these simulation tools are computation speed and the adverse effects of numerical dispersion on computed composition path. For aquifer and coalbed settings there are also several simulation tools available. The capabilities of some of them are reviewed in the paragraphs that follow.

TOUGH2 is a numerical simulator for non-isothermal flows of multicomponent, multiphase fluids in one-, two-, and three-dimensional porous and fractured media²⁰. TOUGH2 was originally developed for geothermal reservoir engineering, nuclear waste disposal and hydrology. There are several simulators in the TOUGH2 family that include physical mechanisms appropriate to CO₂ sequestration in aquifers, including TOUGHREACT/ECO2 (includes transport of aqueous liquid and vapor phases by advection, chemical reactions for dissolved species and minerals, and molecular diffusion in both liquid and gas phases), ChemTOUGH (implicit formulation that allows larger time steps but requires substantially more memory), and TOUGH2-FLAC3D (couples TOUGH2/ECO2 with FLAC3D which models rock and soil mechanics). This family of simulators generally makes use of the equilibrium assumption: components equilibrate rapidly among whatever phases are present. An exception is made for mineral dissolution and precipitation, which can be modeled as in local equilibrium or subject to a kinetic model.

NUFT³⁰ is an integrated software package containing five application specific modules, for the simulation of multiphase and multicomponent flow and reactive transport within a wide range of subsurface environments. The code can model multiphase advection, diffusion, dispersion, relative permeability, and kinetically controlled fluid-mineral reactions. The feedback between transport and geochemical reactions can be modeled by dependence of the permeability on porosity changes due to reactions. PVT properties of CO₂ and water are calculated from equation of state formulations. The SUPCRT92 software package is used for calculation of fluid mineral equilibria³¹. It provides standard state thermodynamic data and equilibrium constants for a wide range of minerals, gases, and aqueous species over a wide range of temperatures and pressures.

FLOTRAN³² describes coupled thermal-hydrologic-chemical processes in variably saturated, nonisothermal, porous media in three dimensions. FLOTRAN describes systems involving two-phase fluid flow and multicomponent reactive chemical transport involving aqueous, gaseous, and mineral species. FLOTRAN includes separate modules that handle the mass and energy transport and the reactive transport. FLOW solves the mass conservation equations for water and gas and energy. TRANS solves mass conservation equations for a multicomponent geochemical system. Effects of capillary, gravity, and viscous forces are included, as are energy transport by convection and conduction. The equilibrium assumption is made for chemical reactions, with kinetic representations available for mineral dissolution and reaction. Changes in porosity and permeability can be represented.

STOMP³³ is a computer model for simulating subsurface flow and transport. Solute transport, radioactive decay, and first-order chemical reactions modeled, following the solution of the coupled flow equations. Reactions and transport are coupled to the flow by accounting for changes in host rock porosity and permeability. An equation of state for CO₂ is included that handles a wide range of temperatures and pressures to 800 bars. Options appropriate to sequestration include H₂O-CO₂-NaCl, H₂O-CO₂-NaCl-Energy, H₂O-CO₂-CH₄-NaCl, and H₂O-CO₂-CH₄-NaCl-Energy. Extension to account for other geochemical reactions is planned.

The UTCOMP simulator is a three-dimensional, isothermal, equation-of-state compositional simulator³⁴. The simulator can be used to study the effects of physical dispersion, gravity, reservoir heterogeneity, phase behavior, fingering, relative permeability and capillary pressure effects including capillary number, and reactive and partitioning tracers. A maximum of four phases is permitted to co-exist, including one aqueous phase and three hydrocarbon phases. Local thermodynamic equilibrium between hydrocarbon phases is assumed with the exception of rate-limited mass transfer of surfactant between phases, rate-limited mass transfer of hydrocarbons into a flowing gas phase and reactive tracers. UTCOMP was written to simulate enhanced oil recovery, and several modifications are needed in order to simulate CO₂ sequestration. For CO₂ injection into aquifers, phase 2 was used for the aqueous phase, and phase 3 was the gas phase (supercritical CO₂ plus some H₂O as a dense fluid phase). Phase equilibrium in the binary CO₂-H₂O mixtures in each grid block is calculated using the Peng-Robinson

equation of state. The effect of salinity on the solubility of CO₂ in brine is modeled by adjusting the binary interaction coefficients in the Peng-Robinson equation. Henry's law is used to model the solubility of CO₂ in water, including a correction for salinity of the brine.

Coalbed methane (CBM) simulators also model physical mechanisms thought to be important in CBE recovery and CO₂ storage processes: the dual porosity structure of the coal bed, adsorption/desorption of CH₄ at the coal surface, coal matrix shrinkage due to CH₄ desorption, and diffusion of gas from the matrix to the fracture system. Additional physical mechanisms that may play a role in CO₂ storage on coalbeds include: coal matrix swelling due to CO₂ adsorption onto the coal surface, mixed gas adsorption, and diffusion of multiple gas components.

Enhanced CBM simulators that are applicable to CO₂ storage can be divided into two groups: those that use a compositional framework, and those that adopt a black oil framework. In the compositional framework, fluid properties are rigorously modeled based on an equation of state. In the black oil framework, fluid properties are supplied by lookup tables obtained through laboratory work or correlations.

Compositional Framework

PSU-COALCOMP³⁵ is a compositional, dual porosity coal bed methane simulator that accounts for multi-component sorption and transport phenomena. Multicomponent sorption is modeled via an ideal adsorbed solution theory and the Peng-Robinson equation of state. Mass transfer between the matrix and fracture system is defined via a sorption time constant, a lumped parameter that incorporates diffusion time, rate or sorption/desorption and cleat spacing of the coal.

GCOMP a simulator that assumes instantaneous diffusion between the matrix and the fracture systems, allowing reduction of the system to a single porosity system³⁶. Mixed gas adsorption is modeled via an extended Langmuir model. In this approach, the concentration of each gas component is a function of its partial pressure. Geomechanical effects on permeability and porosity are modeled, as is coal matrix shrinkage and swelling due to adsorption/desorption of gases on the coal surface.

SIMED II is a two-phase multicomponent single or dual porosity coal bed reservoir simulator³⁷. The Peng-Robinson equation of state is used to calculate fluid properties. Water phase properties are evaluated internally. Multiphase gas adsorption can be modeled via an extended Langmuir isotherm or an ideal adsorbed solution model. Stress-dependent permeability and porosity can be accounted for through a choice of one of five models. SIMED II also accounts for geomechanical effects associated with injection. A dynamic fracture model represents the initiation and growth of injection-induced hydraulic fractures.

CMG-GEM³⁸ is another multiphase, multicomponent single or dual porosity coal bed reservoir simulator. Phase behavior can be described by either the Peng-Robinson or Soave-Redlich-Kwong equation of state. Shape factors can be used to account for flow

between porosities, and additional transfer enhancements can be used to account for fluid placement in the fractures. Mixed gas adsorption is modeled via an extended Langmuir isotherm, and the corresponding diffusion model can be selected based on either concentrations calculated from adsorption characteristics or based on free gas properties. Stress dependent relative permeability changes and matrix swelling and shrinkage can be included.

METSIM2^{39,40} is a 3D multicomponent, triple porosity coal bed reservoir simulator. This formulation assumes that there is no water present in macropore system, only free gas exists, and its transport is diffusion controlled. This formulation allows for the competitive desorption in coal by specifying different diffusion time constants for the macropore and the micropore systems. Gas properties are calculated using an equation of state. Multicomponent adsorption is described using an extended Langmuir model. METSIM2 is also coupled to a wellbore and rock mechanics simulator, allowing pore pressure dependent permeability functionality.

Black Oil Framework

COMET3 is an extension of COMET and COMET2, developed to model low-rank coal and water saturated gas-shale reservoirs⁴¹. It can model single, dual, and triple porosity approximation of the coal bed system. In the triple porosity system, gas desorbs from the internal matrix, and migrates to the micropermeability matrix and finally to the cleat system where it flows to the wellbore. In this formulation, the micropermeability matrix system also models multiphase effects. This accounts for the establishment of a critical gas saturation in the matrix, which may be responsible for a delay in early time gas production observed in some fields. Desorption and diffusion is explicitly modeled. COMET3 can model multiple gas components and accounts for different diffusion rates of the components. An extended Langmuir isotherm is used to model mixed gas adsorption. Pore volume compressibility accounts for stress-dependent porosity and permeability changes. A differential swelling model based on laboratory experiments accounts for swelling attributed to non-CH₄ components of the gas.

ECLIPSE-100⁴² is a black oil simulator with additional features for modeling CBM. A dual porosity system is used to model the coal bed system. This simulator is only able to handle two gas components, and therefore it is not able to model an ECBM process with flue gas injection. Compositional effects between CO₂ and CH₄ are handled by introducing a "solvent" phase. Adsorption is described by the Langmuir isotherm. Eclipse-100 can account for coal shrinkage and compaction effects.

The simulators currently available for aquifer and coalbed storage of CO₂ are very capable, with many physical mechanisms represented. They will continue to be very useful for exploring the interplay of physical mechanisms for computational grids of limited size, but they are subject to significant limitations for application at field scale. Conventional finite-difference compositional simulations, even with relatively small numbers of components, are too slow to handle high-resolution representation of the spatial distribution of permeability at field scale, and when coarse computational grids are used instead, they are badly affected by numerical diffusion, which can alter

calculated composition paths in a way that affects calculated performance significantly. Hence, they are probably not suitable for routine simulation of field-scale flows at grid resolutions sufficient to capture the effects of preferential flow paths created by reservoir heterogeneity, especially if the impact of variability in the permeability distribution is to be assessed. For screening of sites, assessment of areas invaded by CO₂, or rapid exploration of the impact of injection well placement, simulation tools that are significantly more efficient, but necessarily more limited in the mechanisms represented, are appropriate. One approach, the use of streamline methods, is demonstrated next for two of the geologic settings, gas reservoirs, and aquifers. In the section that follows, we also consider the time scales for dissolution of CO₂ in brine in an aquifer and for the equilibration of gas adsorption in a coal bed, summarize work to examine the cooptimization of CO₂ storage and performance of an oil recovery process, and we report results of coal adsorption experiments.

Results

Compositional streamline methods are based on the idea that the flow can be represented as a series of one-dimensional solutions for multiphase, multicomponent flow along each streamline, with the locations of the streamlines capturing the effects of permeability heterogeneity. In reservoir flows that are dominated by heterogeneity, streamlines move little, and hence streamline locations need be updated only occasionally. In those settings, the streamline approach can be orders of magnitude faster than conventional finite difference computations because the largest computational cost is associated with solving the pressure equation for the streamlines. Effects of gravity segregation and capillary crossflow are not represented in the basic streamline approach, a significant limitation for some reservoir settings. Several investigators have shown that it is possible to represent effects of gravity and capillary pressure in streamline computations by operator-splitting techniques. This approach is reasonable as long as very frequent streamline updates are not needed. Frequent streamline updates are subject to errors that arise from mapping and remapping streamlines, and they eliminate the speed advantage of the approach.

Combined CO₂ Storage and Condensate Vaporization

CO₂ injection into a gas reservoir is a process that can be modeled well by a streamline calculation. The viscosity contrast between injected gas and the gas and condensate in place in the reservoir is small (and the mobility ratio is favorable), and density differences are also relatively small, so streamlines change location slowly compared to the rate at which composition fronts move. The local equilibrium assumption (that fluid phases present at a given location are in chemical equilibrium) is also reasonable for this setting.

To test the use of streamline simulation for CO₂ injection in a gas reservoir in which condensate dropout had occurred, we compared streamline simulations with results of ECLIPSE-300 simulations for the same system. In this example, we did not include effects of gravity segregation or capillary crossflow. Analysis of the scaling of these crossflow phenomena suggested that capillary effects were small enough to be neglected,

while gravity effects somewhat larger but still small enough that testing the use of the streamline in the absence of a representation of gravity segregation was reasonable⁴³.

Displacement of a 13-component system was considered. Fluid properties and equation-of-state characterization for the fluid system are reported by Jessen and Orr¹. The analytical solution for one-dimensional displacement of this fluid system by pure CO₂ is shown in Figure 13. As the injected CO₂ propagates through the porous medium, it vaporizes condensate, creating a bank of hydrocarbon liquid at the leading edge of the transition zone. The analytical solution is compared in Figure 13 with a series of finite difference simulations for the same problem, with grid resolutions of 100, 500, 1000, and 5000 grid blocks. Comparison of the numerical and analytical solutions indicates that for this compositional problem, the numerical dispersion present in the FD solutions does not resolve the condensate bank unless a very fine grid is used. It is unlikely that use of such fine grids would be attempted in field-scale compositional simulations because the computation times required would be unacceptably large.

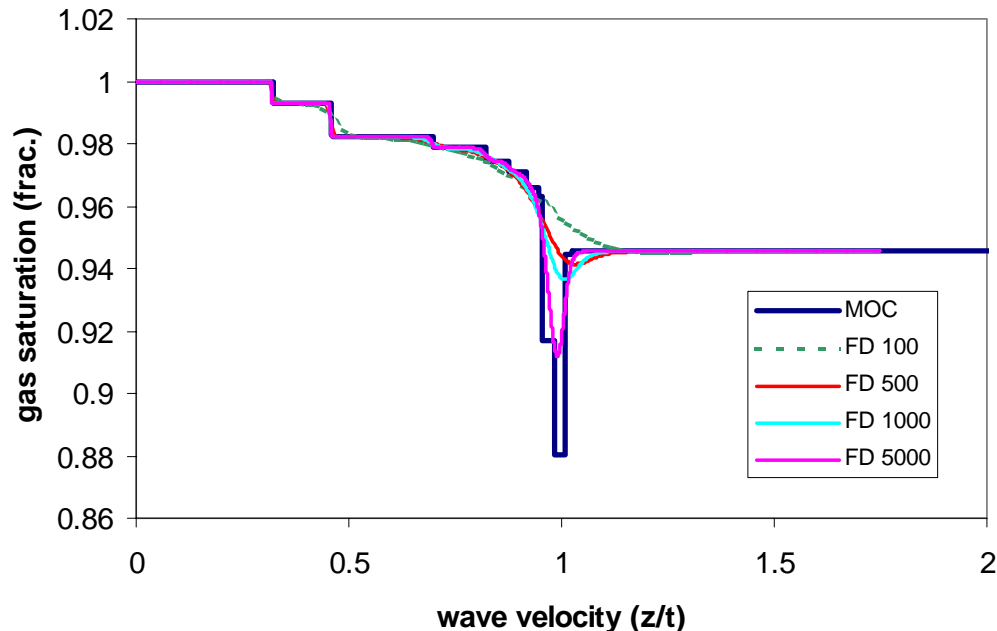


Figure 13: Comparison of analytical solution for 1D displacement of a 13-component gas condensate system by pure CO₂.

Three finite difference simulations, using identical permeability fields, were performed to assess the magnitude of gravitational effects in this displacement:

- Permeability field oriented vertically, injection at a rate advance of 1.4 *m/d* (low rate case).
- Permeability field oriented vertically, injection at a rate of advance of 2.8 *m/d* (high rate case).

- Permeability field oriented horizontally, injection at a rate of advance of 1.4 m/d.

Predicted recoveries and GORs for these simulations are compared to those for a corresponding streamline simulation in Figure 14. Almost no difference is observed among the simulation results for the different orientations and injection rates, an indication that neglecting the effect of gravity for this flow situation is reasonable.

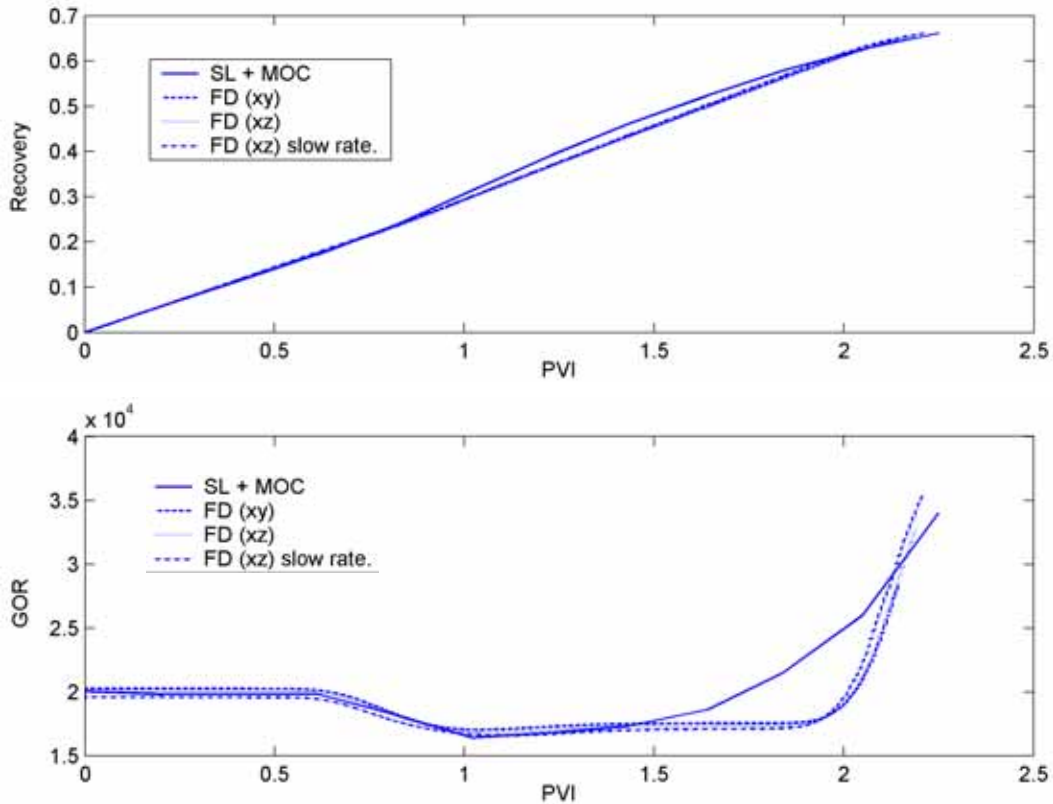


Figure 14: Recovery and GOR predictions for 2D displacement simulations.

Between 0.9 PVI and 1.95 PVI, a separation between recovery predicted by the streamline approach and the finite difference simulations is observed. The maximum separation occurs near 1.4 PVI. This difference is due to the production of the condensate bank resolved in the analytical solution but not in the finite difference computations. In this grid, the resolution between injector and producer is 200 grid blocks. In the finite difference simulations of the 1D displacement shown in Figure 13, this resolution was inadequate to capture the effect of the condensate bank. As injection continues, the difference in recovery between the two methods converges to a similar value. Once breakthrough occurs in the streamline method, injection gas cycles through the reservoir, making the displacement increasingly inefficient. Numerical dispersion in the finite difference method smears the front of the displacement, artificially increasing the sweep efficiency in low permeability regions. The velocity of the front is also reduced, delaying breakthrough, as indicated by the difference in GOR between the two methods at later times.

A 3D sector model representing a multi-well gas injection scheme was simulated. The permeability field and well locations for this displacement are shown in Figure 15. Corresponding recovery and total CO₂ storage curves for the sector model are shown in Figure 16. Breakthrough occurs slightly earlier when the displacement is simulated using streamlines. Again, this is related to formation of high flow zones once the displacement front reaches a producer. CO₂ bypasses condensate in the upswept areas resulting in a lower recovery, but high local displacement efficiency in the swept zones. In the FD simulation, dispersion creates a larger reservoir area contacted by the injected CO₂ while the local displacement efficiency in parts of the swept zones is fairly low. The trade-off between sweep efficiency and local displacement efficiency results, for this case, in a higher recovery prediction by the FD simulation, which may very well be artificially optimistic. While the finite difference method and streamline method represent two end members of process recovery (due to low dispersion effects in a condensate displacement), it is likely that the dispersion-free solution used in the streamline calculation more accurately predicts process recovery. The lower sequestration capacity (Figure 16) predicted by the streamline approach is again due to the lower sweep efficiency, a conservative estimate in this example.

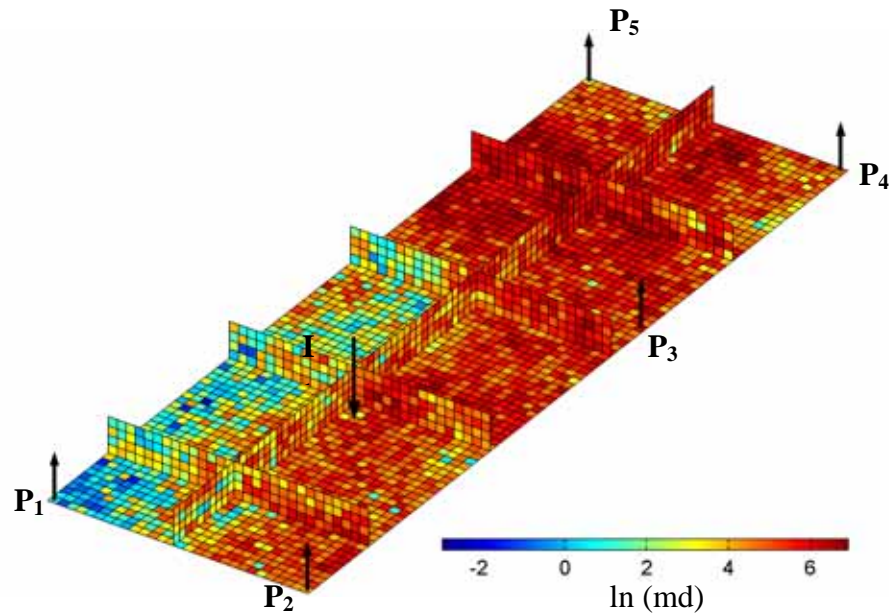


Figure 15: Permeability field and well locations for a 3D sector displacement.

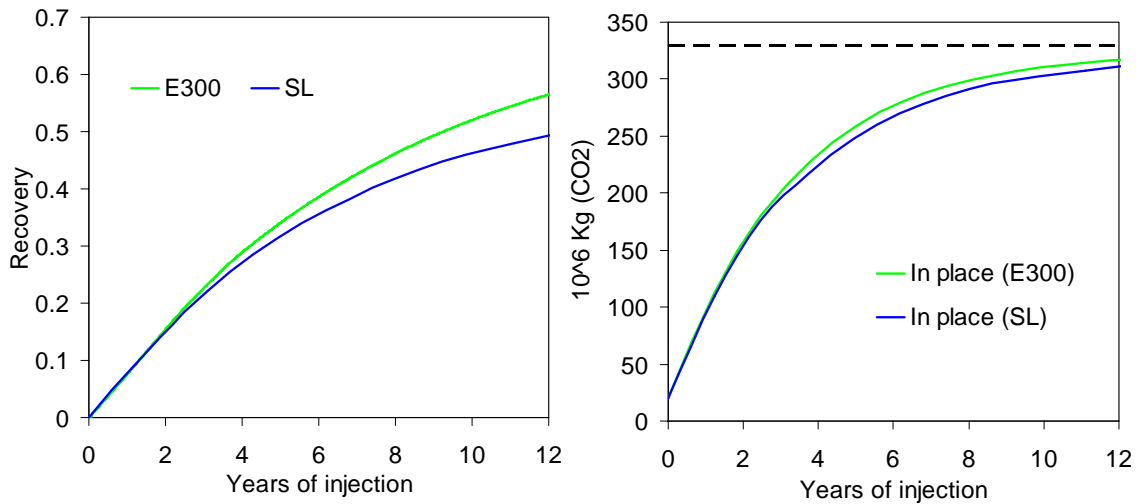


Figure 16: Recovery and sequestration capacity predictions for 3D displacement simulations.

Simulation times of compositional finite difference and streamline simulations are summarized in Table II. Speed-up factors observed were on the order of 10^2 - 10^3 . These are dependent on system size. Computational time in a streamline simulation scales approximately linearly with model size, while that of a finite difference method scales approximately as the third power of the number of grid blocks. Therefore, the ratio of times is approximately the square of the number of grid blocks. As the number of active grid blocks simulated increases, speed-up factors increase approximately quadratically.

Table II: Comparison of FD and SL simulation times.

Model Size	FD (s)	SL (s)	Speed Up Factor
5,000	7406	14	499
13,500	38991	24	1624
5,774	4446	19	234
600,000	N/A	1914 (for 1 PV injected)	

For field scale simulation, where the number of gridblocks can be on the order of millions, streamline simulation is the only method currently fast enough to simulate a sequestration project in a reasonable amount of time. Figure 17 shows the results of an optimization study to increase sequestration capacity of a field scale CO₂ injection scheme. Sequestration capacity was optimized by changing injection well location and the number of injector wells. The reservoir model contained over 500,000 active grid blocks. Injection of 1 PV was simulated.

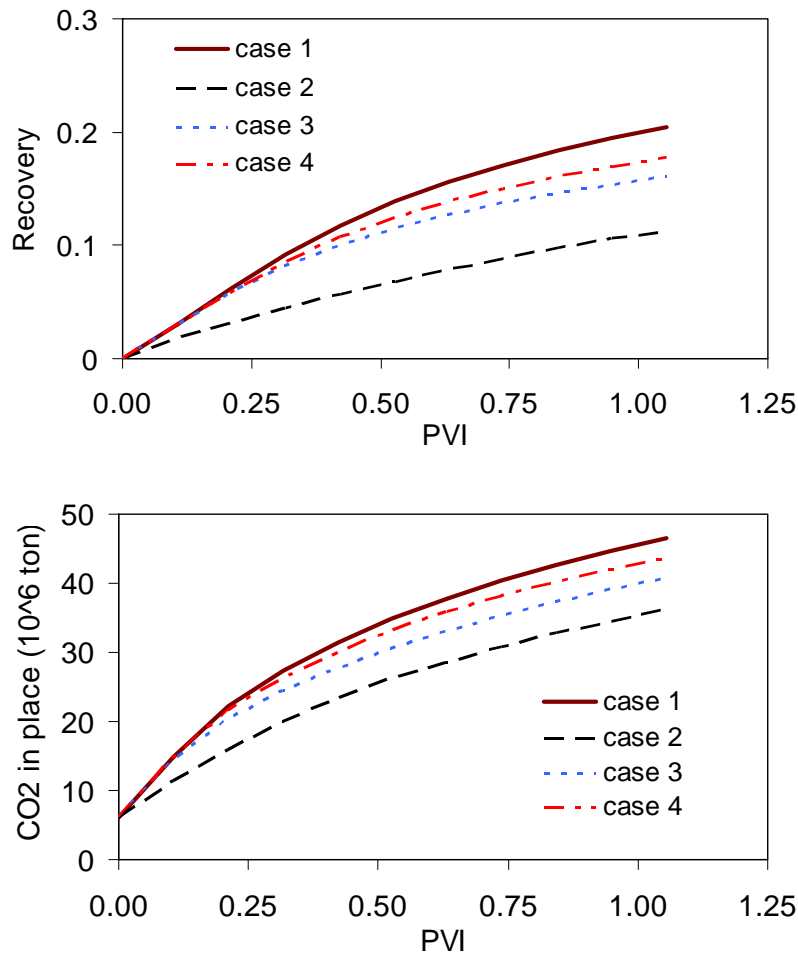


Figure 17: Field scale optimization study to maximize production and sequestration capacity. Reservoir model had over 500,000 active grid blocks. Run time of each streamline simulation was less than 10 minutes.

Cooptimization of CO₂ Storage and Enhanced Oil Recovery

Previous work demonstrated that the design of combined EOR and sequestration operations differs significantly from the design for EOR alone. For pure EOR, the objective is to maximize oil recovery, while injecting minimum CO₂, and this is typically accomplished by injecting water in some version of a water-alternating gas process. In combined sequestration and EOR, oil recovery and the amount of reservoir volume filled with CO₂ are both to be optimized. Last year's report summarized our efforts in cooptimization (see also Cakici⁴⁴)

To examine further the cooptimization question, we used a realistic 3D, heterogeneous, and stochastic reservoir description including a 15-component reservoir fluid. These computations were performed using ECLIPSE-300. The reservoir shape is anticlinal, and it is bounded by faults and an aquifer. There are four injectors near the flanks of the reservoir and 4 producers near the crest. The oil is relatively heavy

(24°API), and pure CO₂ is not miscible in the crude oil at reservoir pressure. A well control scheme was implemented in the simulator that actively shuts in producers with large gas to liquid producing ratios. This scheme allows gas injection without any water injection. Water injection frustrates cooptimization efforts by filling pore space that could otherwise be utilized for sequestration. Control of wells in this fashion allows the same amount of oil to be produced as in an optimized WAG process (with pure CO₂ as the injectant) while simultaneously storing about 2.5 times as much CO₂ as compared to the WAG.

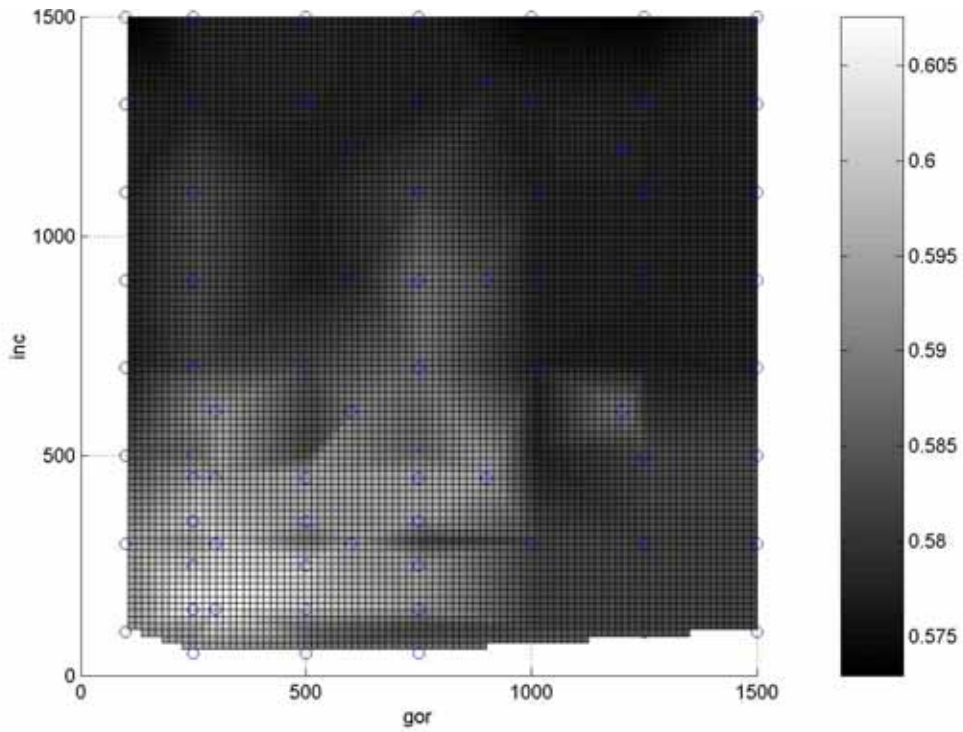
Despite these promising results, questions existed as to whether the well-control scheme was robust and whether the results obtained with the well control were overly sensitive to the distribution of heterogeneities in the reservoir model. The parameters used to operate the production well are producing gas-oil ratio, injection pressure, and an increase in the allowed producing gas-oil ratio each time a producer is allowed to flow. The initial producing gas-oil ratio and the increment to the gas-oil ratio were chosen in an *ad hoc* fashion. The sensitivity of performance to values of the allowed gas-oil ratio and its increment were examined through further simulation.

Figure 18 presents the results for the sensitivity analysis of pure CO₂ injection by plotting the variation in the net cumulative recovery, Figure 18a, and reservoir utilization functions, Figure 18b. The y-axis is the producing gas-oil ratio where the production well is first shut in, whereas the x-axis is the increment made to the producing gas oil ratio each time an injection well reaches maximum pressure (350 *bar*), and producers must be opened to prevent overpressurization of the reservoir. Gray shading represents relatively low values of recovery or utilization, and white represents relatively greater values.

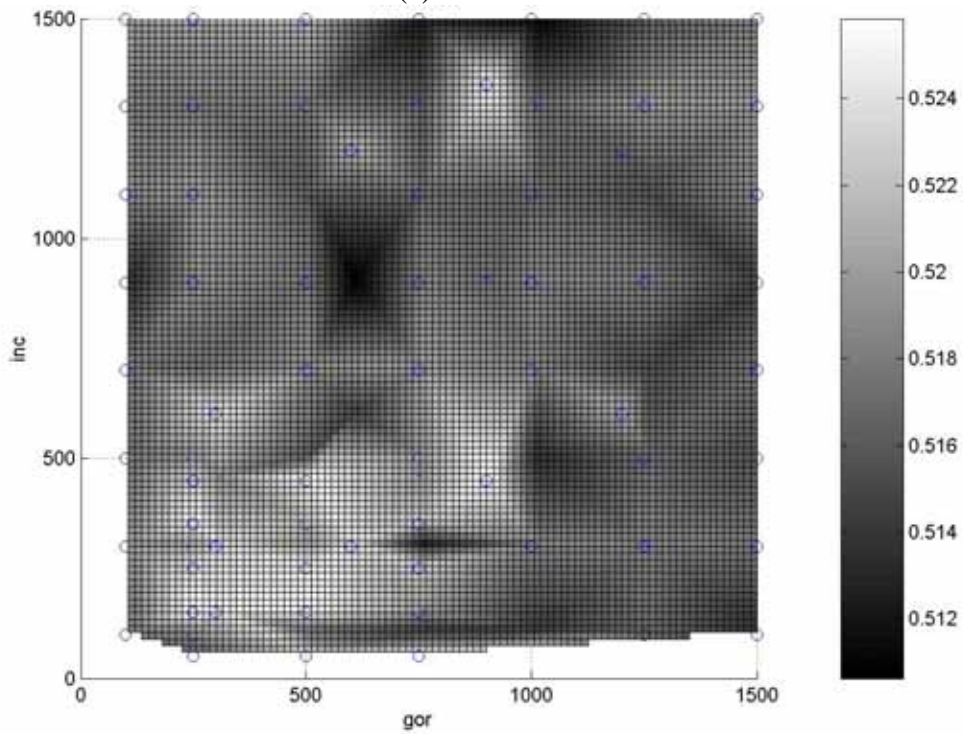
On the one hand, Figure 18 teaches that optimal well control is obtained when the gas-oil ratio where the well is first shut in is set to just slightly above the solution gas-oil ratio (that is the solubility of gas in the oil). This allows control of gas flow at just about the time that gas breaks through to the injection well. Similarly, the results show that increment to the producing gas-oil ratio should be made as small as practical to obtain the best performance.

On the other hand, these results also show that performance of the well-control scheme does not depend critically on control parameters. Note the variations in maximum and minimum values. Differences in recovery and utilization among "best" and "worst" parameters settings differ by 6% to 14%. Thus, the sensitivity analysis indicates that producing gas-oil ratio and injection pressure are robust control parameters. This well-control strategy does not appear to require a high degree of parameter tuning to obtain beneficial results.

Similarly, the sensitivity of results obtained with the well-control scheme was examined as a function of the distribution of permeability within the 3D reservoir model. The injection scenarios include: pure CO₂ injection, WAG with 0.01 PV slugs of CO₂



(a)



(b)

Figure 18: Sensitivity of (a) net cumulative recovery and (b) reservoir utilization results to well-control parameters. Pure CO₂ is injected into 3D reservoir model.

and water, CO₂ injection with well control, and solvent gas (2/3 CO₂ and 1/3 C₂) injection with well control. Results showed that the oil recovery increased or decreased from model to model, but the best performing production scenario for any given reservoir model is well-controlled injection of solvent. With respect to reservoir utilization, well control with pure CO₂ injection sequesters the most CO₂. WAG does lead to different sorting of the performances among the reservoir models; however, these deviations from the reference case do not change the conclusion that the well-controlled cases are preferred for cooptimization.

Time Scales for CO₂ Dissolution in Brine

At the pressures and temperatures encountered in saline aquifers, the injected CO₂ will form a buoyant gas phase, which will therefore migrate back towards the surface unless migration is inhibited by a geological barrier to vertical flow. To understand whether and if so how much CO₂ might be available to flow vertically, we need to understand how long the injected CO₂ will be mobile. Therefore, we need to understand trapping mechanisms that prevent upward migration by CO₂ and the time-scales over which they operate. If the CO₂ gas phase moves due to its buoyancy or is displaced by invading brine, gaseous CO₂ may be trapped as an isolated residual CO₂ phase. This mechanism will be referred to below as residual trapping. CO₂ has a modest solubility in the aqueous phase, the aqueous CO₂ increases the density of the brine slightly⁴, and therefore brine containing dissolved CO₂ will sink rather than rise. We will refer to this trapping mechanism as solution trapping. Figure 19 shows sketches of possible configurations of CO₂ in an aquifer.

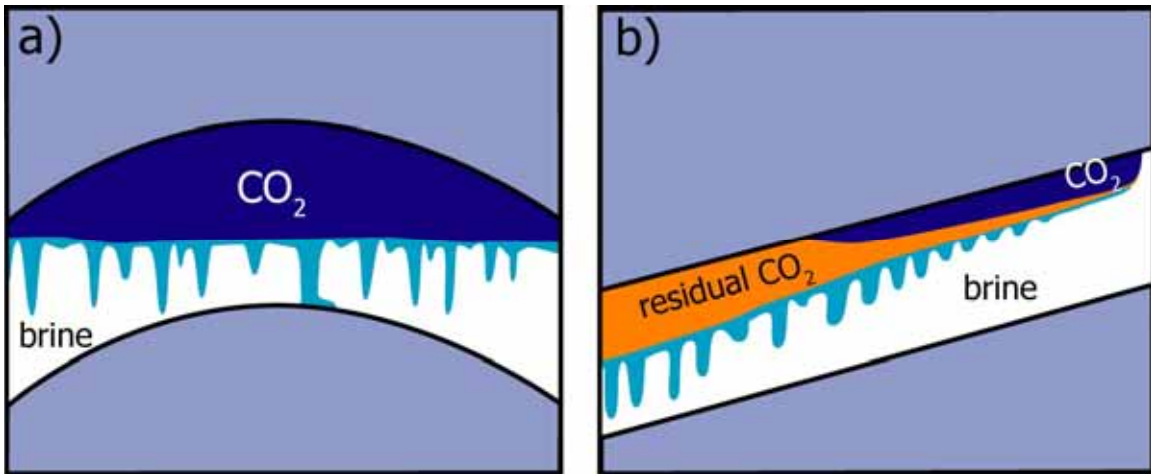


Figure 19: Schematic of CO₂ dissolution in two aquifers. The mobile CO₂ gas phase is dark blue, the dissolved aqueous CO₂ is light blue, residual CO₂ is orange, and the brine is not colored. a) CO₂ gas is held under a structural trap. Dissolution of CO₂ into the brine reduces the CO₂ phase volume. b) The CO₂ gas phase migrates along the top of a sloping aquifer, and leaves behind a region of residual CO₂. In this case both dissolution and residual CO₂ saturation contribute to the decrease of the mobile CO₂ phase.

Reactions of dissolved CO₂ with cations in the brine may ultimately lead to the precipitation of minerals, depending on brine chemistry and aquifer mineral content.

These geochemical reactions have rate constants low enough⁴⁵ that mineralization reactions will not contribute volumetrically to the trapping of CO₂ in the first several hundred years. However, small changes in porosity due to precipitation may significantly decrease the permeability and help to trap the CO₂ plume dynamically. Residual and dissolution trapping are therefore the likely mechanisms that decrease the amount of mobile CO₂ within the first several 100 years. Residual trapping will only be important if the CO₂ plume moves through the aquifer, and water invades zones containing gas, a likely event as CO₂ from the gas phase transfers to the brine. Dissolution trapping will contribute when CO₂ gas phase is in contact with the brine.

Convection Enhanced Dissolution

At the interface between gaseous CO₂ and the brine, CO₂ dissolves into the brine. This dissolution is fast enough that it can be considered to be at equilibrium. The rate of CO₂ dissolution is therefore determined by the transport of CO₂ away from the interface. In the absence of advection, the aqueous CO₂ has to diffuse away from the interface. Ennis-King and Paterson⁴ have estimated that the minimum time until a given CO₂ layer is dissolved by diffusion alone as

$$\tau_{Diff} \sim \frac{\alpha L^2}{D}, \quad (1)$$

where $\alpha \sim 10$ is the ratio of the density in the gas phase CO₂ to the mass of CO₂ per unit volume of brine containing dissolved CO₂, $D \sim 10^{-9} \text{ m}^2/\text{s}$ is the molecular diffusion coefficient, L is the thickness of the initial layer of gaseous CO₂. For $L \sim 10 \text{ m}$ the minimum time for dissolution of all CO₂ is of the order of 1 million years. Advective transport of CO₂ away from the interface could increase the rate of CO₂ dissolution and decrease the dissolution time scale by orders of magnitude.

Ennis-King and Paterson⁴ report an increase of brine density with increasing aqueous CO₂ concentration. This allows convective transport of CO₂ away from the interface due to buoyancy-driven convection. They argue that the minimum time for dissolution in this case is given by the time it takes for the heavy fingers to propagate a distance αL . Assuming a gravitational velocity $u_g \sim g \Delta \rho k / \mu$ where g is the gravitational acceleration, $\Delta \rho$ is the density difference, k is the permeability and μ is the viscosity of the brine, the time for convective mixing is at least

$$\tau_{mix} \sim \frac{\alpha L \mu}{g k \Delta \rho}. \quad (2)$$

For common aquifers, this time scale is on the order of $10^4 - 10^5$ yrs, up to two orders of magnitude shorter than the diffusive time scale. Gravity-driven convection may therefore enhance CO₂ dissolution significantly, if it occurs. Convection will only be an effective transport mechanism if fingers of dense CO₂ can migrate significant distances before diffusion eliminates the concentration and hence the density difference. For a

disturbance with distance d between adjacent fingers, the diffusive time scale for cross-finger transport is

$$\tau_{cross} \sim \frac{(d/2)^2}{D}, \quad (3)$$

so that the length scale of vertical finger propagation is at least

$$L_f \geq u_g \tau_{cross} = \frac{gkd^2 \Delta\rho}{4\mu D} = \frac{10 \cdot 10^{-13} \cdot 5}{4 \cdot 6 \cdot 10^{-4} \cdot 10^{-9}} d^2 \approx 2d^2. \quad (4)$$

Depending on the wavelength of the disturbance d , L_f may be smaller or bigger than the required distance for dissolving all CO₂ given by αL .

A mathematical analysis of the instability of the diffusive boundary layer can determine the circumstance under which the diffusive boundary layer will become unstable, subject to the assumptions and boundary conditions used, of course, and give some insight in the initial length scale of the disturbances. Ennis-King and Paterson have presented such a stability analysis of the diffusive boundary layer at the interface between the gaseous CO₂ and the brine⁴. They also performed numerical simulations with the TOUGH2 code²⁰ that show propagation of CO₂ fingers over tens of meters in 10³ to 10⁴ years. However, the simulations were affected significantly by numerical dispersion, and the numerical grid had a similar or larger length scale than the instabilities in their simulation results. We have reproduced and checked their stability analysis and translated it back into physical space.

To analyze the stability of the boundary layer mathematically, Ennis-King and Paterson have assumed an infinite, homogenous, horizontal layer of depth H . The gaseous CO₂ layer supplying the aqueous CO₂ is neglected. This is a reasonable assumption, because the gravitational instability is between two miscible phases, brine and heavier brine with dissolved aqueous CO₂. They further assume that the density change is small enough so that it can be neglected in all terms except the gravitational term, this is also called the Boussinesq approximation. The governing equations are therefore:

$$\nabla \cdot \bar{u} = 0, \quad (5)$$

$$\bar{u} = -\frac{\underline{K}}{\mu} \cdot (\nabla P - g\rho \hat{e}_z), \quad (6)$$

$$\phi \frac{\partial C}{\partial t} + \bar{u} \cdot \nabla C = \phi D \nabla^2 C, \quad (7)$$

where $\bar{u} = (u, v, w)$ is the Darcy velocity, P is the pressure, \underline{K} is a diagonal permeability tensor that may be anisotropic ($k_x = k_y \neq k_z$), μ is the viscosity of the fluid, $\rho(C)$ is the density of the fluid, g is the gravitational acceleration, C is the concentration of aqueous

CO₂, ϕ is the porosity of the porous medium, and D is the coefficient of molecular diffusion of aqueous CO₂ in water. The initial state that is considered is supposed to represent the aquifer some time after CO₂ injection has stopped, and the system has come to rest. The initial condition is therefore $\bar{u}(t=0, \bar{x}) = 0$, and initially there is no dissolved CO₂ in the brine, hence $C(t=0, \bar{x}) = 0$. The boundary conditions are no penetration for the vertical component of the velocity $w(z=0, t) = w(z=H, t) = 0$ and the concentration has mixed inhomogeneous boundary conditions $C(z=0; t) = \frac{\partial C}{\partial z} \Big|_{z=H} = 0$. Choosing the following characteristic scales $C_c = C_0$, $t_c = H^2/D$, $x_c = y_c = H/\gamma^{1/2}$, $z_c = H$, $u_c = v_c = \phi D/(H\gamma^{1/2})$, $w_c = \phi D/H$ and pressure is scaled by $P_c = \mu\phi D/k_v$, where $\gamma = k_z/k_x$ is the permeability anisotropy, the dimensionless governing equations are

$$\nabla \cdot \bar{u} = 0, \quad (8)$$

$$\bar{u} = -\nabla P + \gamma Ra C, \quad (9)$$

$$\frac{\partial C}{\partial t} + \bar{u} \cdot \nabla C = \gamma \nabla_H^2 C + \frac{\partial^2 C}{\partial z^2}, \quad (10)$$

where $\nabla_H^2 = \frac{\partial^2}{\partial x^2} + \frac{\partial^2}{\partial y^2}$, and $Ra = \frac{g\Delta\rho k_h H}{\mu\phi D}$ is the Rayleigh-Darcy number. The governing equations only depend on two parameters, the permeability anisotropy γ and the Rayleigh-Darcy number Ra . The initial and boundary conditions for the advection diffusion equation admit the following transient base state solution,

$$C_b(t, z) = 1 - \frac{4}{\pi} \sum_{n=1}^{\infty} \left(\frac{1}{2n-1} \sin((n-1/2)\pi z) e^{-(n-1/2)^2 \pi^2 t} \right). \quad (11)$$

To study the stability of this base state solution, we introduce small perturbations in concentration and velocity. First we linearize the perturbed equations and subtract the base state. Then we make the plane wave approximation for the shape of the disturbances and obtain two coupled partial differential equations for the amplitude of the velocity and concentration perturbations $\hat{w} = \hat{w}(z, t)$ and $\theta = \theta(z, t)$:

$$\frac{\partial^2 \hat{w}}{\partial z^2} - s^2 \hat{w} + \gamma s^2 Ra \theta = 0, \quad (12)$$

$$\frac{\partial^2 \theta}{\partial z^2} - \gamma s^2 \theta - \frac{\partial \theta}{\partial t} - \hat{w} \frac{dC_b}{dz} = 0. \quad (13)$$

Here s is the wave number of the two-dimensional perturbations. The system of PDE's is solved numerically, by reducing them to a system of ordinary differential equations (ODE's) using the Galerkin method and then solving the system of ODE's numerically.

The system of coupled ODE's for the Galerkin coefficients a_l of the concentration disturbance is

$$\frac{da_m}{dt} = A^{-1} \underbrace{(B - \gamma Ra C E^{-1} D)}_{G_{ml}} a_l, \quad (14)$$

where $G_{ml} = G_{ml}(t)$ is a full $N \times N$ matrix, and its coefficients are functions of time. Finally, the average concentration and velocity disturbance can be calculated from the Galerkin coefficients.

The resulting solutions confirm the well-known result that all perturbations decay below a critical Rayleigh-Darcy number. In the context of aquifer sequestration it is useful to fix all physical properties of the aquifer and to think of the Ra number as proportional to the depth H of the layer. For convection to occur, the aquifer needs to exceed a certain critical depth. This depth increases with anisotropy, but is generally less than 15 m for $\gamma \geq 0.01$, $\Delta\rho = 5 \text{ kg/m}^3$, $g = 10 \text{ m/s}^2$, $\mu = 6 \cdot 10^{-4} \text{ Pa s}$, $D = 10^{-9} \text{ m}^2/\text{s}$, $\phi = 0.2$, and $k = 10^{-13} \text{ m}^2$. All results discussed below will be in terms of this choice of parameters.

An interesting result of this analysis is that above the critical Rayleigh-Darcy number all perturbations decay initially before they start growing exponentially as shown in Figure 20. There is an initial period of stability before the onset of the convective movement. The longer this critical time is, the longer it will take until mixing enhances the CO₂ dissolution rate. Ennis-King and Paterson observed, and we confirm, that the critical time is a strong function of the permeability anisotropy, as shown in Figure 21. The critical time increases from tens of years to hundreds of years as the anisotropy changes from $\gamma = 1$ to $\gamma = 10^{-2}$. Even in the worst case this is only a small fraction of the minimum time estimated above to dissolve all CO₂ by convective mixing, and therefore only delays it. Finally the stability analysis gives us information about the wavelength λ of the perturbations that grow initially. As for depth greater than the critical depth, the wavelength asymptotically approaches a constant value for a given permeability anisotropy. This wavelength increases with increasing anisotropy; our results show a stronger increase compared with those of Ennis-King and Paterson. The initial wavelength is only an indication of the wavelength established in the fully nonlinear system. A rough estimate for the depth of finger penetration is obtained by setting $d = \lambda/2$ in the scaling law for L_f . Using our results $\lambda(\gamma = 0.1) \approx 20 \text{ m}$ so $d \approx 10 \text{ m}$, and hence the penetration depth of the fingers is roughly on the order of $L_f \approx 200 \text{ m} \approx \alpha L$. This scaling argument suggests that the instability is strong enough to propagate fingers far enough to mix the dissolved CO₂ with a large enough amount of water to dissolve all CO₂.

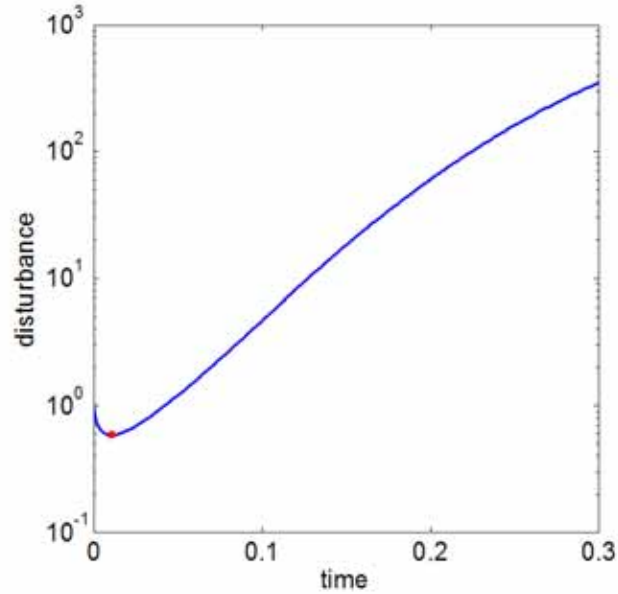


Figure 20: The vertical axis shows the average magnitude of the concentration perturbation vs. dimensionless time. The evolution for the disturbance corresponding to a particular wavelength and at a Ra number above the critical Ra number is shown. The disturbance first decays, reaches a minimum, and then grows exponentially. The time required to reach the minimum is the critical time for the onset of the instability.

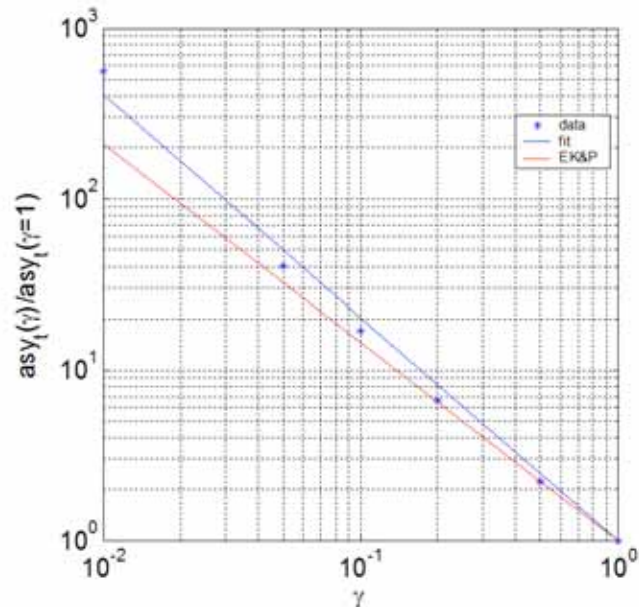


Figure 21: The vertical axis is critical time for a given permeability anisotropy normalized by the critical time for an isotropic aquifer. This ratio increases as the anisotropy increases. The red line shows the power law fit to the numerical results from Ennis-King and Paterson⁴, the blue stars are our numerical results, and the blue line is the power law fit to our results.

The analysis discussed here is based on a flow geometry and a set of simplifying assumptions that may not reflect actual aquifer settings. In a typical aquifer the injected CO₂ will flow preferentially through high permeability paths. The interfacial tension between CO₂ and brine will be high, and the viscosity of CO₂ will be significantly lower than that of brine, so CO₂ will displace water inefficiently and vice versa. All of these physical mechanisms will act to increase the volume of brine contacted and the area of contact, which should increase the rate of dissolution. In addition, most aquifers will not be strictly horizontal, and hence there will be some gravity-driven flow in the up-dip direction. This flow will also increase the area of contact. On the other hand, permeability heterogeneity can restrict vertical flow, which would increase dissolution time. Investigation of the interplay of heterogeneity, dissolution, gravity segregation of injected CO₂, slow density-driven convection in the brine phase, and diffusion will require high-resolution numerical solutions for the appropriate combination of mechanisms, a task that is next on our agenda. While the streamline approach demonstrated above can handle effectively the injection period, it is not the appropriate choice for examining the interplay of diffusion, convection, and possible chemical reactions that occur in the long term.

Streamline Simulation of CO₂ Injection in Saline Aquifers

In the previous section, the convection-enhanced dissolution mechanism for trapping CO₂ in an aquifer was discussed. This section focuses on the effect of residual gas trapping on the ability of a given CO₂ plume to migrate upwards and potentially leak to formations above the injection zone.

As CO₂ is injected into an aquifer, the interplay of various parameters including density and viscosity of brine and CO₂ at the prevailing temperature and pressure in the formation will determine the potential for the injected CO₂ to migrate upwards in the formation due to buoyancy. Also, the permeability variations within the aquifer and the presence of any potential flow barriers (shales) will play an important role in the trajectory of the injected CO₂.

Potential sites for CO₂ sequestration in saline aquifers span a wide range of parameter values and accordingly, some of these must be more optimal for long term storage than others. The variation of the viscosity of pure water (similar in behavior to the brine of a saline aquifer) over a fairly narrow range of temperatures can be significant, as Figure 22 shows.

Within the temperature and pressure intervals of probable injection sites, the viscosity of water can vary from 1.25 cp at low temperatures to 0.25 cp at high temperatures. From Figure 22, the modest variation in viscosity with pressure suggests that pressure effects on water viscosity can be neglected in modeling studies as a reasonable approximation. At higher temperatures, the brine in the formation will be more mobile than at lower temperatures, and hence for a given set of rock properties, CO₂ will face less resistance to flow as it displaces brine, suggesting that gravity effects can be more important at these conditions provided that the density difference between brine and CO₂ is sufficiently high. Figure 23 illustrates the variation in CO₂ density with pressure at 313 K and 363 K

(for additional isotherms, see McHardy and Sawan⁴⁷. If CO₂ is injected at supercritical conditions, the density can vary from ~200 kg/m³ at low pressures to ~800 kg/m³ at high pressures. The density of water/brine is a relatively weak function of temperature (~1000 kg/m³ at low temperatures to ~960 kg/m³ at the normal boiling point), and it is a weaker function of pressure. Hence a significant upward driving force due to density differences

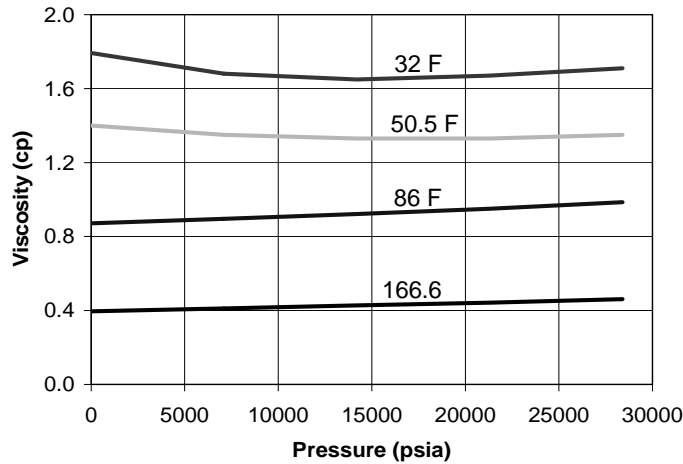


Figure 22: Dependence of water viscosity on pressure and temperature⁴⁶.

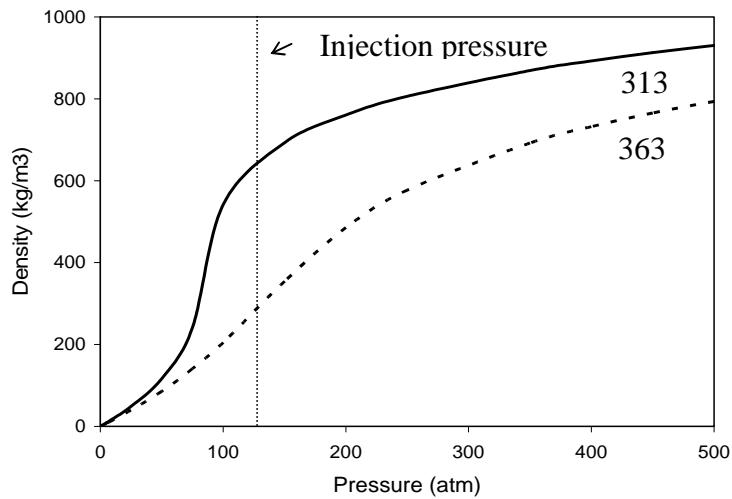


Figure 23: Dependence of CO₂ density on pressure and temperature.

can exist in warm aquifers, where the mobility of water is high relative to cold aquifers, in which the upward migration of CO₂ can be limited by the lower mobility of the brine.

To estimate the magnitude of gravity-to-viscous forces in a given sequestration setting, we adopt the formulation suggested by Zhou *et al.*⁴⁸, who define the ratio of gravity to viscous forces by the dimensionless group, N_{gv} :

$$N_{gv} = \frac{g\Delta\rho LK_{av}}{Hv\mu_w}. \quad (15)$$

In Eq. (1), $\Delta\rho$ is the density difference between the injected and the resident fluid, L is the displacement length, K_{av} is the average absolute permeability in the formation, H is the height of the formation, v is the injection velocity and μ_w is the viscosity of the initial fluid in the formation (water). To map out the potential range of sequestration scenarios, Table III reports estimates of low and high values of the individual components of Eq. (1) and the corresponding value of the gravity to viscous number N_{gv} .

Table III: Gravity and viscous forces in aquifer sequestration.

Estimate	$\Delta\rho$ (kg/m ³)	L (m)	H (m)	K_{av} (mD)	v (m/day)	μ_w (cp)	N_{gv}
High	800	1E5	200	1000	10	1	33.5
Low	200	1E3	10	1	0.1	0.2	0.84

From the reported estimates of high and low values of the gravity to viscous forces, we find that depending on the temperature and pressure of the aquifer (as well as the permeability and injection rates), we might expect to see a full range of flow patterns within the various aquifers from gravity-dominated flow to viscous-dominated flow. In the following subsection, we investigate the effect of changes in fluid properties with temperature and the significance of residual trapping.

To test our qualitative scaling argument, a series of example calculations was performed. All were done with the Stanford compositional streamline simulator, CSLS. The simulator describes the phase behavior of the CO₂-brine system by a modified version of the Peng-Robinson equation of state². Special care must be taken to account properly for the mutual solubility of CO₂ and brine. Our approach follows the modifications outlined by Yan *et al.*⁴⁹. Temperature-dependent shift parameters are used to ensure accurate prediction of phase densities. Simulation of CO₂ injection in the formation shown in Figure 24 was performed at two temperatures to evaluate the impact of variations in fluid properties.

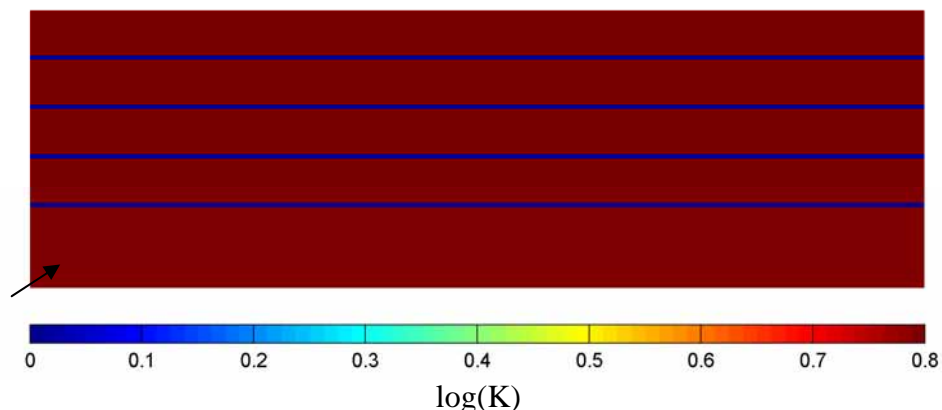


Figure 24: Permeability field used in simulation study.

The formation is a 6000 m by 189 m cross-sectional area of an aquifer consisting of 5 high-permeability (3000 mD) sand compartments separated by low-permeability shales (3 mD). The porosity of the sands is 35% whereas the porosity in the shales is 3.5%. The simulation grid is 100*62, a bit on the coarse side, but sufficient to investigate variation in flow patterns with temperature. Corey type relative permeability curves were used with an irreducible brine saturation of 0.2. The same relative permeability curves were used for the sandstones and shales. The first example simulation was performed at 313 K (40C). The sequestration process was simulated for two years for four values of the critical gas saturation (0, 0.05, 0.1 and 0.2). Figure 25 reports the fluid distribution at the end of the injection phase.

As the residual gas saturation is gradually increased, the tendency for the CO₂ to follow the preferential flow paths below the shales decreases. Also, the significance of the gravity override decreases as gas is trapped with increasing S_{gc} . From Figure 25, it is clear that the critical gas saturation can play an important role in preventing the free CO₂ from migrating to the top of the formation. Comparison of the locations of the gas fronts in the top ($S_{gc} = 0$) and bottom panels ($S_{gc} = 0.2$) of Figure 24 indicates that the increase in S_{gc} must result in an increase in the amount of CO₂ that is dissolved in the brine. Figure 26 reports the concentration maps for two of the displacements illustrated in Figure 25. It confirms the observation that although a smaller volume of the brine is contacted by CO₂ at high S_{gc} , the concentration of CO₂ in the contacted brine is higher than for $S_{gc} = 0$. For comparison with the second set of displacement calculations, we note that the ratio of gravity to viscous forces for the low temperature displacements is estimated to $N_{gv} = 4.1$.

In the second set of displacement calculations, the temperature of the aquifer was set to 363K (90C). Accordingly, the viscosity of the brine is reduced from ~0.653 cp to ~0.276 cp, while the viscosity of CO₂ declined from 0.05 to 0.025 cp. In this displacement the gravity-to-viscous ratio was $N_{gv} = 21.1$. Figure 27 demonstrates that there is a more significant impact of gravity segregation at the higher temperature. As for the low temperature calculations, the sequestration process was repeated for four levels of

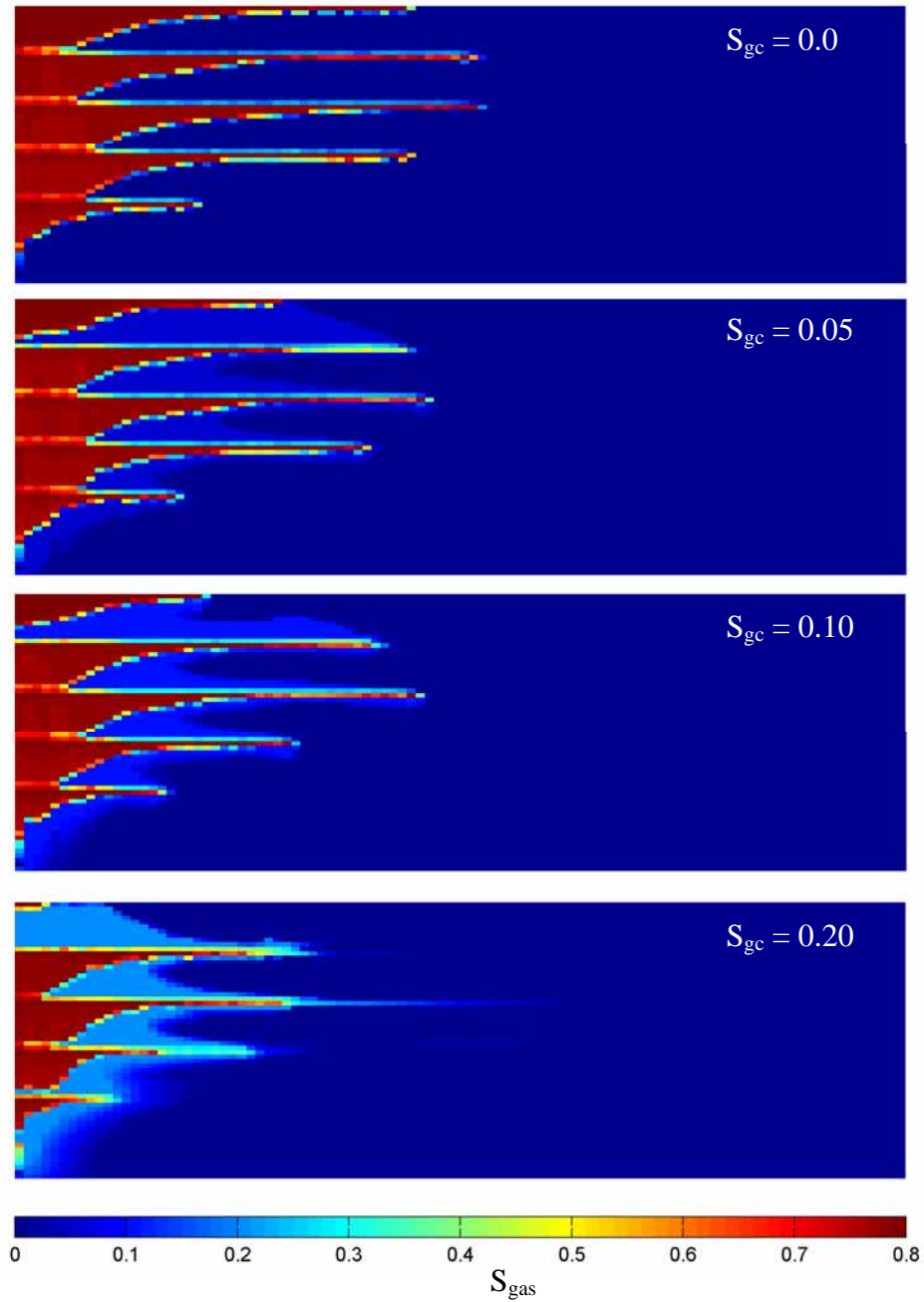


Figure 25: Gas saturation after two years of injection ($T = 313K$).

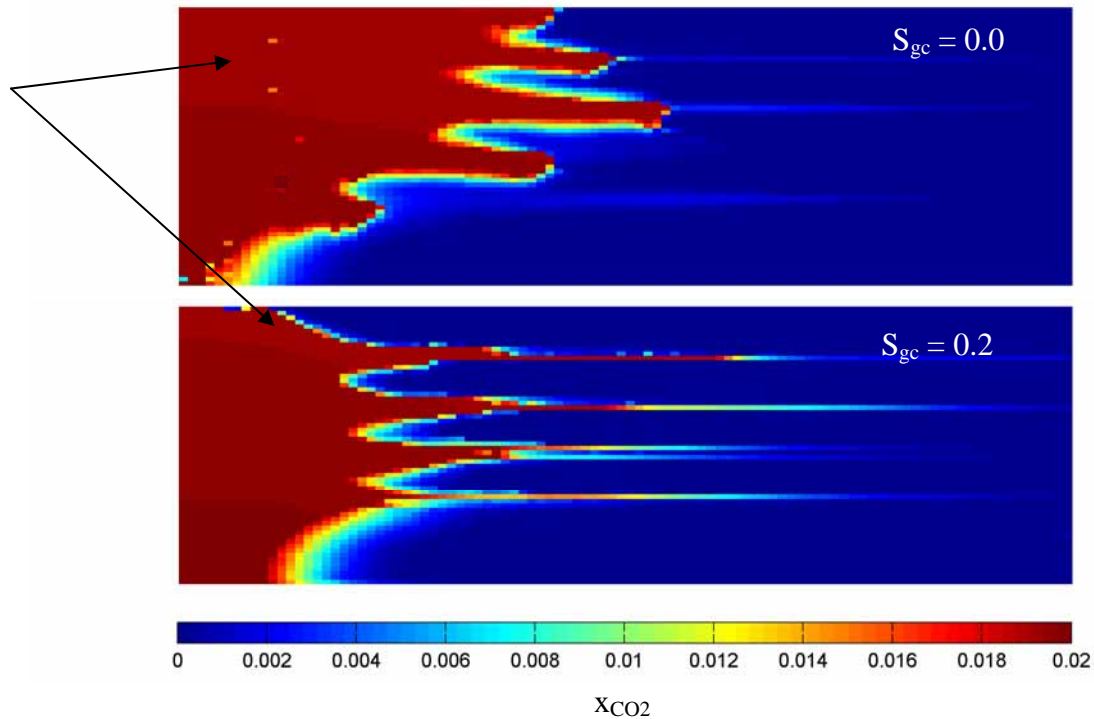


Figure 26: Mole fraction of CO₂ dissolved in the brine (T = 313K)

critical gas saturations, S_{gc} (0, 0.05, 0.1 and 0.2). The results of the simulations after two years of injection are reported in Figure 27. For the high temperature (high mobility of brine) we find a significant increase in the predicted gravity override. Four factors contribute to the increase in gravity segregation: (a) the gas phase is less restricted to flow in the vertical as well as the horizontal direction due to the decrease in brine viscosity, (b) the density difference between the injected CO₂ and the brine has increased as the CO₂ now has a density of $\sim 260 \text{ kg/m}^3$ as opposed to the low temperature displacement where the injected CO₂ had high density of $\sim 670 \text{ kg/m}^3$, (c) at the higher temperature, the solubility of CO₂ in the brine is lower resulting in a larger volume of mobile low-density gas in the formation, and (d) the ratio of water viscosity to CO₂ viscosity increases at the higher temperature, resulting in a lower local displacement efficiency.

The simple scaling arguments and examples presented here, demonstrate the impact of the fluid properties in an aquifer injection process on the tendency of the injected CO₂ to migrate upwards in the formation. The examples also confirm the utility of the streamline simulation approach for this problem. Numerical solutions were used along streamlines, which were updated periodically, as gravity segregation shifted streamlines. Each simulation took about ten minutes of computation time. Those simulations can be performed at low enough cost in computation time that the interplay of heterogeneity,

trapping, and solubility can be explored in detail for the injection period of an aquifer storage project.

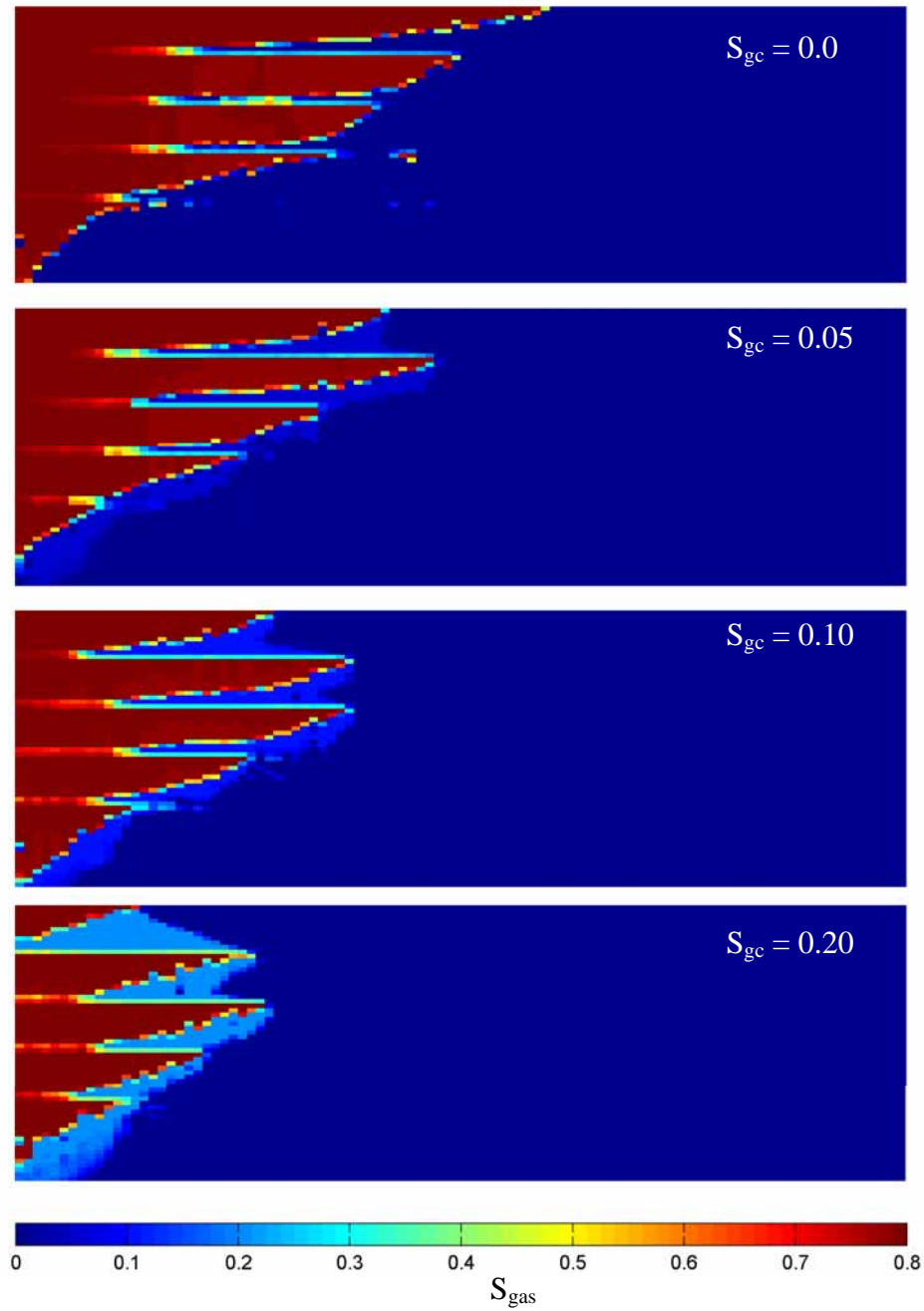


Figure 27: Gas saturation after two years of injection ($T = 363K$).

Time Scales for Coalbed Sequestration

Enhanced coal bed methane (ECBM) recovery combined with CO₂ storage is one option for sequestration of CO₂. Flow through coalbed reservoirs occurs in a network of subparallel face cleats orthogonally intersected by butt cleats. For a mature, high-rank coal, typical cleat aperture is approximately 0.1 mm, and typical cleat spacing is 1-2 cm^{50,51}. When CO₂ is injected, it flows through the cleat system and diffuses into the matrix. Preferential adsorption of CO₂ causes adsorbed CH₄ to desorb. The desorbed CH₄ then diffuses through the matrix to the cleat system, where it flows to the production well and is produced. Diffusion through the matrix is controlled by concentration gradients, while flow through the cleat system is controlled by pressure gradients. The rate of production from coalbed reservoirs is controlled by the slower of these two processes. In this section, we consider the question of whether it is appropriate to model field-scale flow in a coalbed with an assumption of local chemical equilibrium between coal and gas or whether some more complex model is required.

The following simple scaling analysis examines the effect of diffusion transport in the cleat and matrix systems. In cases where convection dominates, the local equilibrium assumption is reasonable. If the local equilibrium assumption can be made, then the cleat network controls flow through coal bed reservoirs, and the details of matrix diffusion effects need not be represented explicitly.

Cleat System. Flow in the cleat system can be described by the convection-dispersion equation shown in Eq. 16, which describes the concentration of injected gas in the fracture system, C_f . The Peclet number (Pe), defined in Eq. 17, is a ratio of the characteristic time for diffusion to the characteristic time for convection.

$$\frac{\partial C_f}{\partial \tau} + \nabla \cdot C_f - \frac{1}{Pe} \nabla^2 C_f = 0, \quad (16)$$

where

$$Pe = \frac{vL_f}{D_f}, \quad (17)$$

and τ is dimensionless time, v is the average flow velocity in the fractures, L_f is the displacement length, and D_f is the diffusion coefficient in the gas phase in the fractures. Large values of Pe characterize convection-dominated flows. For typical ECBM displacements, Pe is very large. For a flow velocity of 0.33 m/d, a flow length of 400 m, and a diffusion coefficient in the gas of 10⁻⁴ cm²/s, for example, the resulting Peclet number is 1.5 x 10⁵. That value is large enough that it is quite reasonable to neglect the effects of longitudinal diffusion in the flow calculation.

Matrix System. In the coal matrix system, we assume that diffusion is the only mechanism of transport. The conservation equation is

$$\frac{\partial C_m}{\partial t} = \nabla \cdot D_m \nabla C_m, \quad (18)$$

where C_m is the concentration of injection gas in the matrix and D_m is the diffusion coefficient in the matrix. Diffusional transport was considered for a dry matrix and a wet matrix. For the dry matrix, diffusion through a single matrix block was considered. The system was reduced to an equivalent spherical system, and a constant diffusion coefficient was assumed. For a spherical coordinate system, Eq. (3) becomes

$$\frac{\partial C}{\partial t} = \frac{D_m}{r^2} \frac{\partial}{\partial r} \left(r^2 \frac{\partial C}{\partial r} \right), \quad (19)$$

with boundary conditions

$$C(r = R, t) = 1, \quad (20)$$

$$C(r, t = 0) = 0. \quad (21)$$

The time required for the average concentration in the sphere to reach 95% was calculated. The resulting diffusion time as a function of effective diffusion coefficient and radius of the sphere is shown in Figure 28. The time required for equilibration depends fairly strongly on the assumed diffusion coefficient. Shi and Durucan⁴⁰ report values, estimated by fitting effluent composition data for pulverized coals, of 5×10^{-8} to $5 \times 10^{-6} \text{ cm}^2/\text{s}$ for micropores and 2×10^{-5} to $7 \times 10^{-4} \text{ cm}^2/\text{s}$ for macropores. Thus, for large diffusion coefficients, equilibration time for all radii of sphere considered is on the order

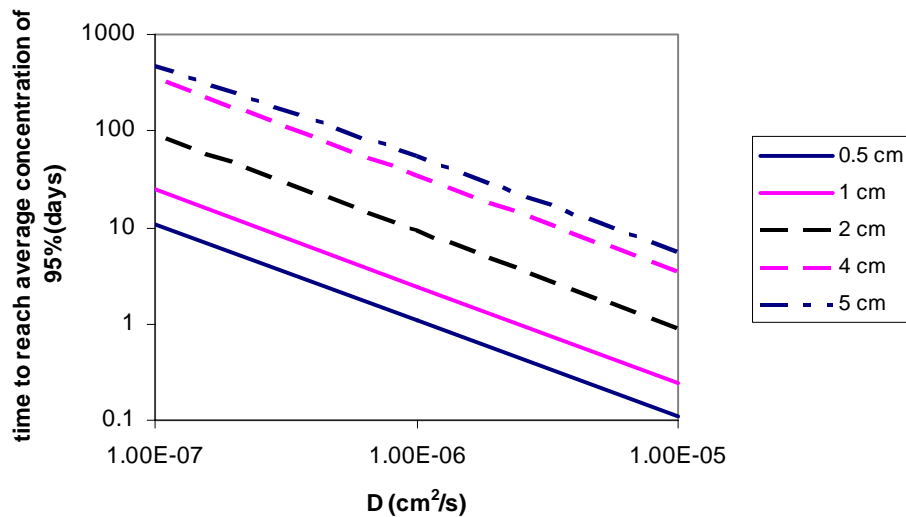


Figure 28: Time required for the average concentration to reach 95% in a sphere of dry coal. Typical matrix size for a mature coal is 1-2 cm.

of days. For small diffusion coefficients, equilibration time is a function of the radius of the system, ranging from a few days for spheres with a 1 cm radius, to months for spheres

with a 5-cm radius. For a high rank coal, where fracture spacings are small, equilibration time is on the order of tens of days for a typical solid diffusion coefficient of $10^{-7} \text{ cm}^2/\text{s}$.

Coal reservoirs are typically water saturated, and the coal surface is water wet⁵³. In this system, for mass transfer between matrix and fracture systems, we assume that gas must diffuse through a thin film of water. The presence of water creates extra resistance to mass transfer. The concentration gradient driving mass transfer in the water phase is relatively low, because the solubility of gas in the water limits the concentration gradient in that phase.

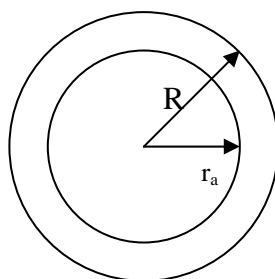


Figure 29: Schematic of a simplified wet matrix system.

For this calculation, the wet matrix was approximated as a spherical film of constant thickness, surrounding the matrix (Figure 29). The time to reach the 99% of the solubility concentration at r_a is presented as a function of diffusion coefficient and film thickness in Figure 30. For the range of thicknesses and diffusion coefficients considered, film equilibration times are very short (on the order of minutes) compared to matrix equilibration times. Diffusion coefficients for CO₂ in water at high pressure are on the order of $10^{-5} \text{ cm}^2/\text{s}$ ⁵². Hence we conclude that for a typical cleat aperture of 0.1 mm, the time required for diffusion through a water film with similar thickness is small compared to the other characteristic times for flow and equilibration.

This simple analysis of diffusion in the cleat and matrix system suggests that diffusion times are short enough that for flow at field scale, it is a reasonable approximation to assume that the fluid in the cleat system is in equilibrium with the solid. If so, then the problem of representing adsorption of CO₂ and other gases in a coalbed revolves around accurate representation of the multicomponent adsorption. If a suitable model of that adsorption is available, it should be possible to take advantage of the speed of streamline simulation techniques for this system.

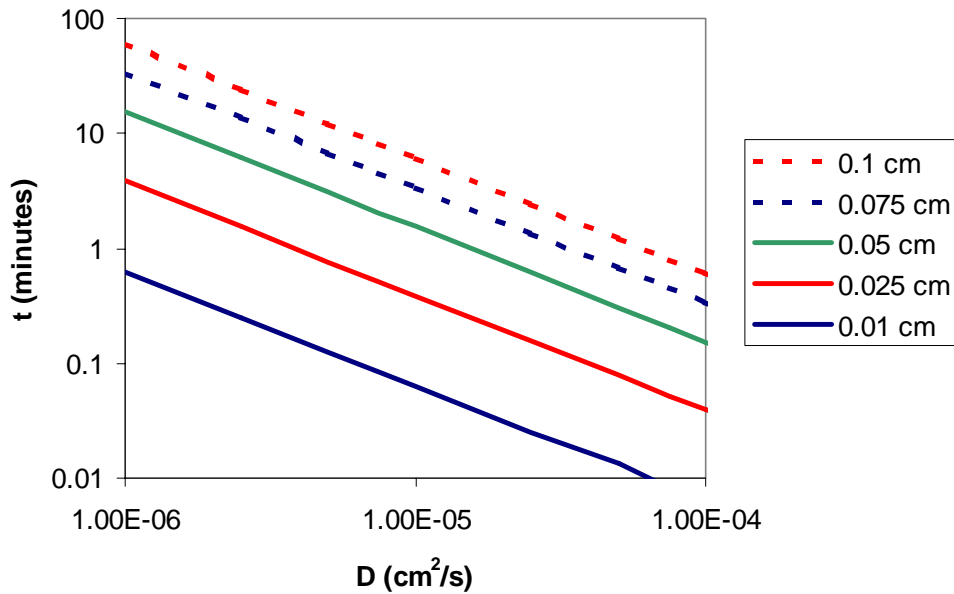


Figure 30: Time required for wet film to reach solubility concentration.

Enhanced Coalbed Methane Recovery and CO₂ Sequestration

The relatively advanced state of knowledge regarding the mechanisms of EOR is not matched for gas injection into coalbeds. Our previous analytical study of the flow of multicomponent gases through dry coal (Zhu *et al.*⁸) revealed the strong coupling between the advance of a gas species and its adsorption properties. It was predicted that coals are capable of separating CO₂ from N₂, among other results. Experimental verification of model predictions appears prudent before adding more detail to the calculations.

An experimental program was begun with the goals of validating prior flow and adsorption predictions as well as developing a database for comparison of more advanced predictions. The apparatus developed is illustrated in Figure 31. The centerpiece is the core holder for holding coal samples that are 4.25 cm in diameter and up to 25 cm long. To date, we have employed crushed (60 mesh) and dried coal samples from the Powder River Basin. The crushed coal is packed to obtain a porous medium with a permeability of 80-100 *md* and a porosity of 0.33. The apparatus is capable of using intact core samples, but no field samples available to us had sufficient integrity to be employed directly.

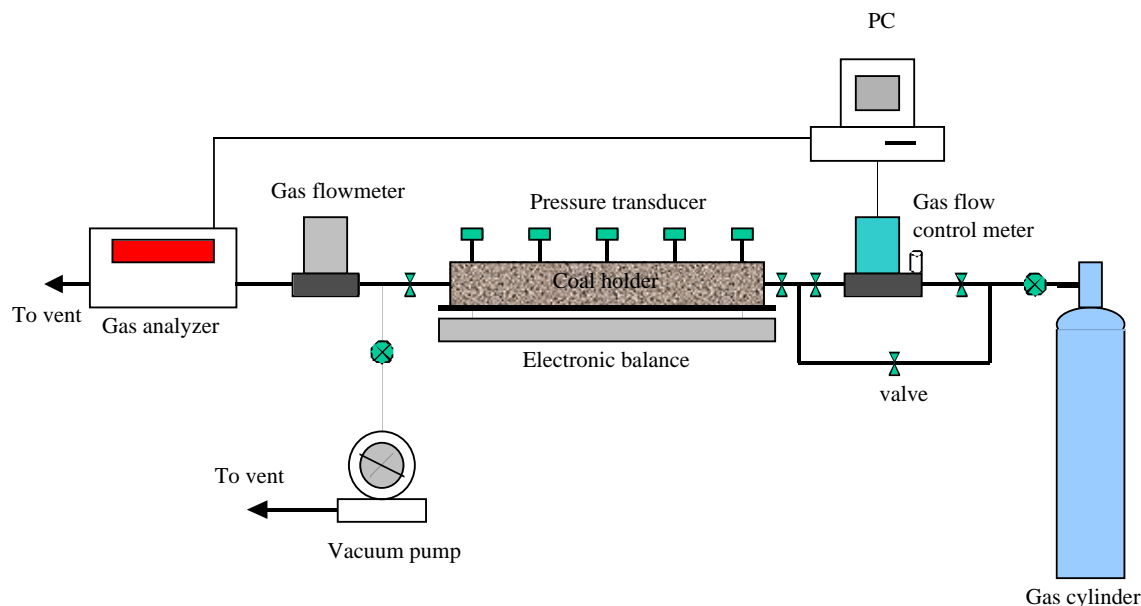


Figure 31: Schematic of experimental apparatus.

Coal surfaces are equilibrated with methane at a given pressure, typically between 500 and 750 psi. The displacement gas is a mixture of CO₂ and N₂, and its flow is metered by a 0-50 SCCM (standard cubic centimeters per minute) mass flow controller. The concentration of gas components (CO₂, CH₄, N₂) in the effluent and at sampling ports along the length of the core is measured with a gas analyzer to $\pm 0.01\%$. The rate of gas production is also measured as is pressure drop along the core. A backpressure regulator maintains the outlet of the system at constant pressure.

A first step in the investigation was the measurement of the adsorption and desorption properties of pure CO₂, CH₄, and N₂ on the coal. Measurement results are given in Figure 32. Several notes are in order. First, CO₂ was the most strongly adsorbing gas. At 800 psi, roughly 3 times as much CO₂ adsorbed as did CH₄ and more than 8 times as much CO₂ adsorbed as did N₂. Second, there was significant hysteresis among adsorption and desorption results. Upon depressurization, coal retained significant volumes of gas. At 220 psi, this coal retained 80% of the CO₂ that had adsorbed at 800 psi. The hysteresis between adsorption and desorption characteristics does not yet have a satisfactory physical explanation. Nevertheless, the difficulty in desorption of CO₂ suggests that coal may be a secure site for CO₂ sequestration.

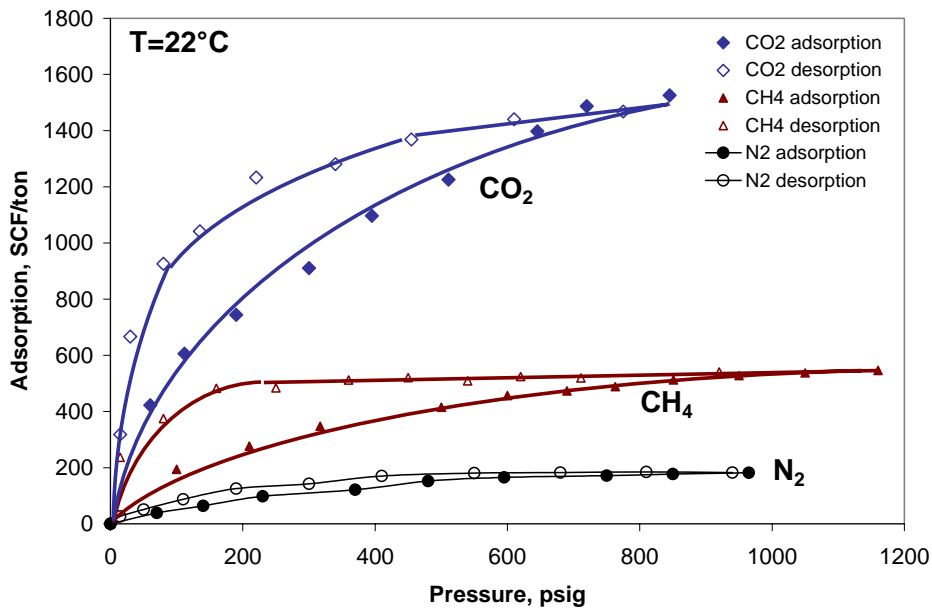
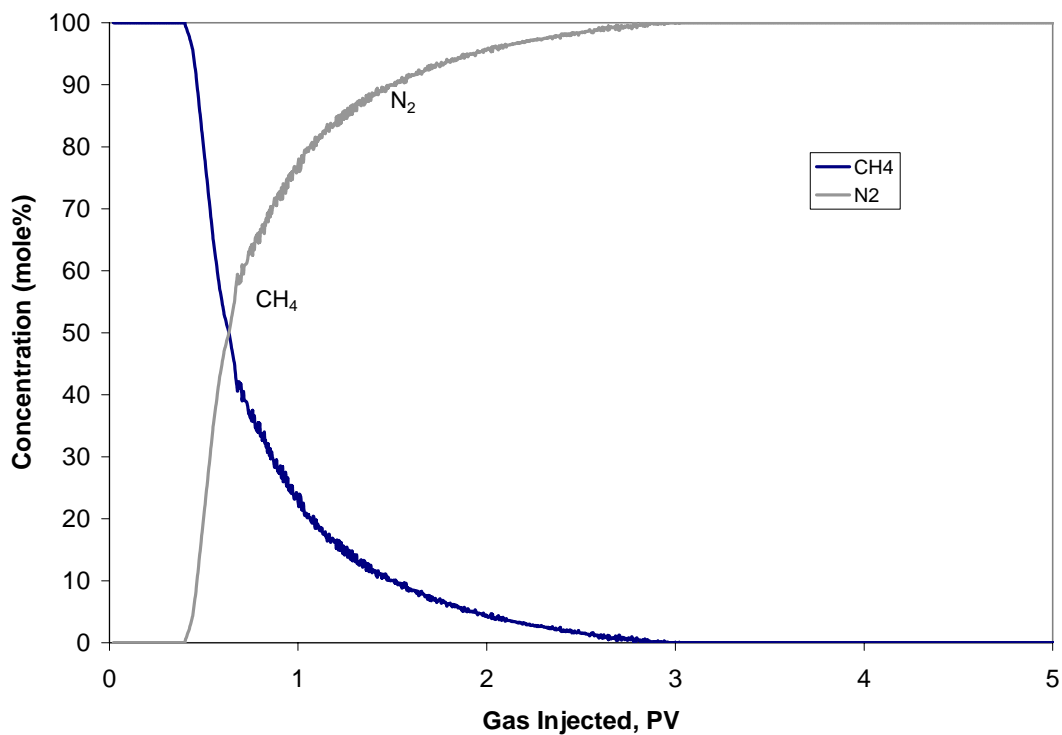


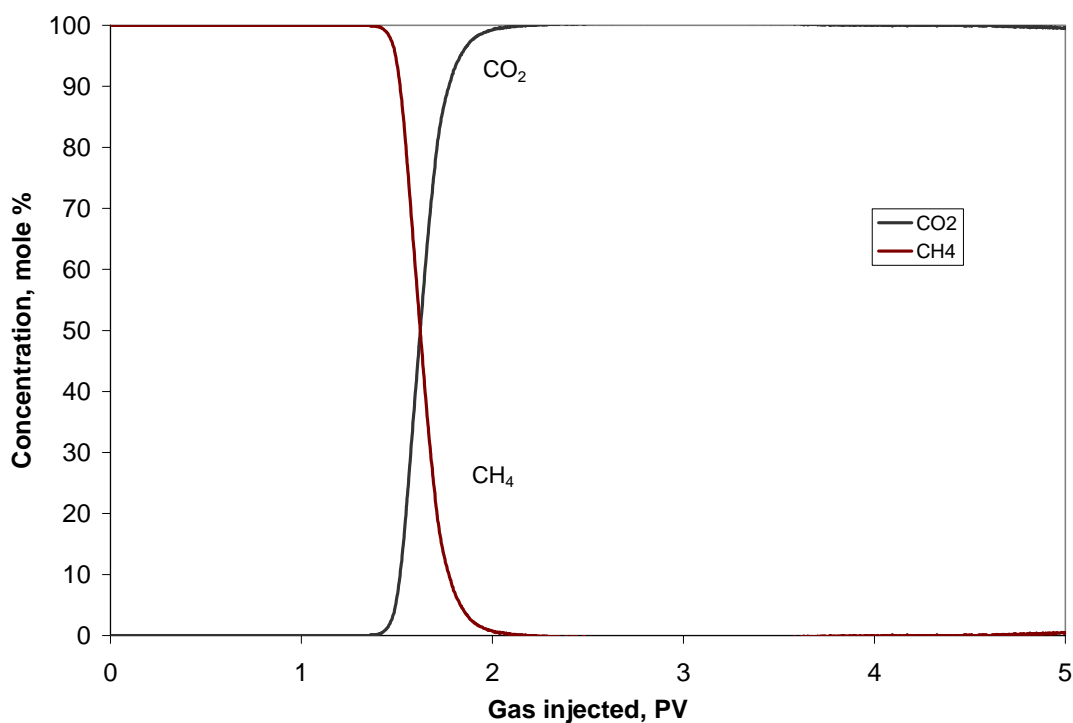
Figure 32: Adsorption-desorption isotherm for gases on crushed, dried samples of Powder River Basin, WY coal at 22°C.

A suite of displacement experiments is underway to be used subsequently to interpret ECBM and sequestration mechanisms and thereby to provide a first step in improving conceptual and mathematical models. Some representative results follow. Figure 33 provides a comparison between pure N₂ and CO₂ as injection gases. The figure shows the composition of gas exiting the coal versus the amount of gas injected in pore volumes (PV) computed at the outlet pressure of the coal. Comparison of Figures 33(a) and (b) shows that injected N₂ broke through to the exit in about 0.4 PV whereas CO₂ did not appear until after 1.5 PV of total gas had been injected. Note also that a significant fraction of the CH₄ produced as a result of N₂ injection was mixed with N₂. About 3 PV of total injection was required to sweep out the CH₄ with N₂. Production of CH₄ as a result of CO₂ injection was virtually complete when CO₂ broke through at 1.5 PV, and there was little production of CH₄/CO₂ mixtures. Permeability of the pack decreased by 34% as CO₂ replaced CH₄. Total recovery of the initial CH₄ in the system was 77% with N₂ injection and 92% as a result of CO₂ injection. With respect to recovery, breakthrough time, and the mixing of injection gas and CH₄, CO₂ is the superior injection gas.

Injection gases with various concentrations of CO₂ and N₂ have also been tested. Figure 34 shows the production profiles resulting from an injection gas with 23.5% CO₂ and the balance N₂. Such a mixture might be similar to a combustion gas enriched in CO₂ but not separated completely. Notably, N₂ broke through at the outlet in roughly 0.4 PV, and its concentration increased rapidly thereafter; however, CO₂ did not appear until



(a)



(b)

Figure 33: Production profiles for pure gas injection into a Power River Basin, WY coal sample: (a) pure N₂ injection gas and (b) pure CO₂ injection gas. The system backpressure is 600 *psi*. Injection rate is 0.5 SCCM.

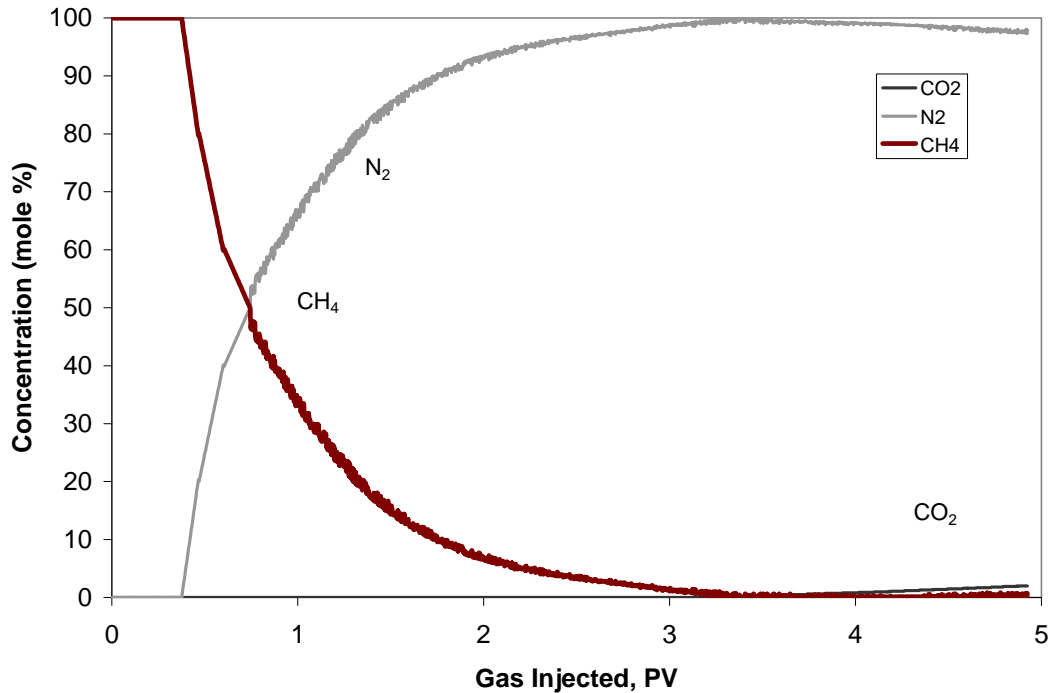


Figure 34: Production profile for gas injection into a Powder River Basin, WY coal sample. Injection gas is 23.5% CO₂ and 76.5% N₂. The system backpressure is 600 *psi*. Injection rate is 0.5 SCCM.

after 3.3 PV of injection and the fraction of CO₂ in the produced gas always remained low. The coalbed effectively separated the N₂ and the CO₂ in the injection gas. The total CH₄ recovery for this experiment was 80%.

Should such laboratory results for injected gas mixtures prove relevant to the field scale, they indicate a clear tradeoff between the compression required to elevate the mixed gas to injection pressure and the cost to separate CO₂ from N₂ on the surface prior to injection. Note that the experiments also suggest that N₂ may have to be separated from produced CH₄ for a significant period of the total production period with either the injection of pure N₂ or a mixture containing significant N₂.

II.3.3 Geophysical Monitoring of Geologic Sequestration

Investigators

Jerry M. Harris, Professor, Geophysics Department; Youli Quan and Tapan Murkeji, Research Associates, Geophysics Department; Martins Akintunde and Chuntang Xu, Graduate Research Assistants.

Background

Subsurface monitoring will be required to provide: (1) early warning of reservoir leaks to address public safety concerns; (2) images of the space-time distribution of injected CO₂ to aid optimization of injection and storage; and (3) input to the safety case analysis expected to be required for a permit and licensing process. Geophysics offers a variety of methods that operate over a wide range of geological environments, reservoir scales, and depths. The challenge is to track the flow of CO₂ while simultaneously monitoring for leaks in a growing subsurface volume. Moreover, a thorough description and predictive simulation of the monitoring capability may be required for the safety case when a site is presented for licensing.

During the initial phase of the study, we developed models that estimate the changes in bulk rock-fluid properties with injected CO₂. We then considered several geophysical monitoring methods, e.g., seismic, electrical, magnetic, electromagnetic, gravity, and surface deformation (Wynn⁵⁴) and performed sensitivity analyses for each. See summary below. The major conclusion of this initial study was that seismic methods provide the most effective and universally applicable technology for subsurface monitoring for the various geologic storage scenarios of coal beds, deep saline aquifers and depleted oil and gas fields. However, seismic imaging, as we know it from the petroleum industry, is too expensive for continuous or repeated long-term monitoring. Our ongoing research is focusing on the development of cost-effective time-lapse seismic imaging techniques that can potentially provide quasi-continuous monitoring and adapt to address safety concerns. We're following the guiding principle that the monitoring effort must decrease with time, barring a reservoir problem, and eventually cease altogether when safe containment is no longer a concern.

Summary of Subsurface Monitoring Options

This section summarizes the results of our scoping study on the applicability of various geophysical methods for monitoring CO₂ sequestration. The details of this study are given in Wynn⁵⁴. He explored the available options for monitoring formations undergoing CO₂ injection. Rock physics models were used to determine the time-lapse changes in relevant physical properties (acoustic, electrical, etc.) for a variety of rock types at the pore scale. These rock physics models were used in a synthetic formation model to estimate field or measurement scale changes. Results from different settings were compared to suggest optimum monitoring techniques for monitoring geologic sequestration. Also examined were the potential uses of each technique for monitoring CO₂ migration, seal integrity, and mass balance. Seismic, electromagnetic, gravitational, and geodetic methods are the four broad types of subsurface geophysical monitoring examined. Direct sampling methods such as monitoring wells have high spatial resolution

but low spatial coverage. Subsurface geophysical imaging techniques generally have high spatial coverage with limited spatial resolution, but have the added benefit of being remote. While a monitoring well would have to penetrate the formation seal to gather meaningful hydrologic data or fluid samples, possibly creating conduits for CO₂ to escape, seismic imaging may be used to image the area of interest without such intrusion.

In seismic monitoring, the changes we may detect are changes in velocity, reflectivity, and possibly attenuation. The bulk of the velocity changes resulting from saturation effects occur with only a small amount of CO₂ in the pore space. For this reason seismic monitoring will be very useful in leak detection and for monitoring CO₂ migration. Seismic monitoring should be able to detect thin layers of CO₂, under favorable circumstances meaning that migration paths should show up in a reflection survey and the presence of CO₂ in overlying zones should be easily detectable. The acoustic velocity of fluids under most reservoir conditions is typically above 1000 m/sec, whereas the velocity of CO₂ is considerably less. Figure 35 shows velocities of CO₂ at different pressures and temperatures. Figures 36 and 37 are examples of wave velocity changes in CO₂ flooded sandstone and CO₂ flooded coal. The velocity change due to CO₂ flooding is significant, which favors the seismic monitoring.

Resistivity surveys are the simplest method of assessing subsurface conductivity. At the large separation distances required for monitoring CO₂ sequestration such techniques will detect only the average changes in the reservoir and may be of too low resolution to be of any use. Another option is crosswell electromagnetic measurements. At the low frequencies necessary to propagate EM waves across field scale distances the resolution is fairly low, and the measurements are strongly affected by the conductivity structure near the source and receiver.

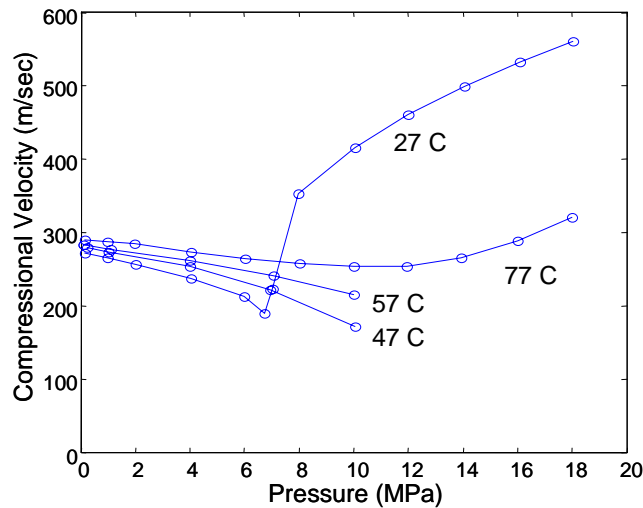


Figure 35: P-wave velocities of CO₂ (Wang and Nur⁵⁵).

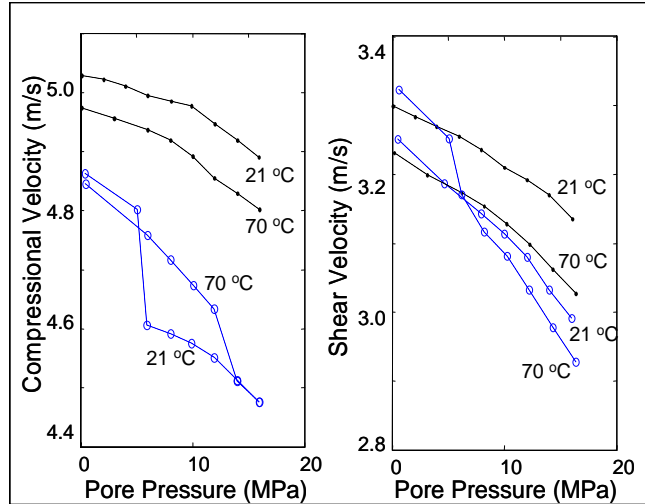


Figure 36: P-wave velocities in hydrocarbon-saturated and CO₂-flooded sandstone. Black lines are isotherms for hydrocarbon-saturated rocks, and blue lines are isotherms for flooded rocks. Confining pressure for the plots is 20 MPa (Wang and Nur⁵⁵).

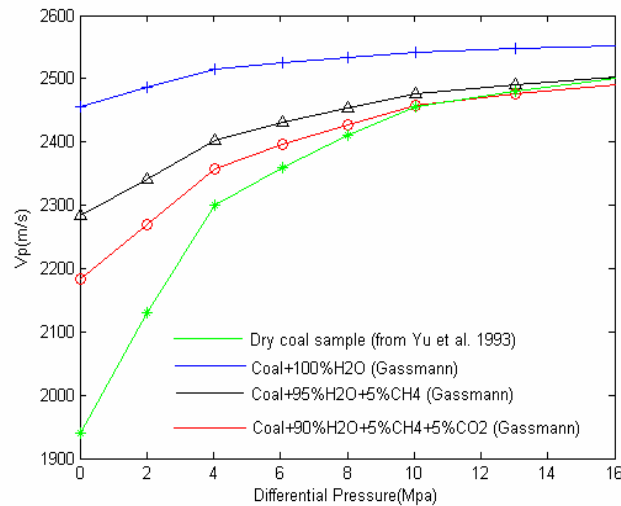


Figure 37: Predicted P-wave velocities in a CO₂-flooded coal from Gassmann's equation (Gassmann⁵⁶) and laboratory data from Yu *et al.*⁵⁷.

Gravity monitoring is only suitable for making very low-resolution mass balance measurement, and that too in shallow formations as the signal falls off inversely with distance squared. Geodetic techniques measure displacements or displacement gradients at the earth's surface. Such techniques are commonly used in the study of earthquakes or volcanoes but may also have limited applications in monitoring CO₂ sequestration under

certain conditions. In a stable tectonic environment, measured deformation over a sequestration site should only be the result of induced pressure changes at depth due to fluid injection. However, surface geodetic techniques, much like gravity, are very low-resolution techniques.

The results of Wynn's⁵⁴ study are summarized in Table IV. Not surprisingly seismic, being a versatile, high-resolution technique has the widest range of uses and is not limited by geologic setting. The SACS project at Sleipner has certainly confirmed the ability of seismic monitoring to track CO₂ in the subsurface.

Table IV: Summary of the usefulness of geophysical techniques by use and setting.

	Seismic	Electromagnetic	Gravity	Deformation
Mass Balance	low res.	low res.	good	good
CO ₂ Migration	good	good	low res.	low res.
Leak Detection	good	good	low res.	no
Geologic Setting	any	aquifers	any	oil and gas
Rock Strength	any (soft better)	any	any	soft
Formation Depth	any	any	shallow	shallow

Adaptive Seismic Monitoring: A New Approach to Time-Lapse Subsurface Imaging

Our proposal for subsurface CO₂ monitoring is to trade the conventional approach of high spatial/low temporal resolution for a new approach providing low spatial/high temporal resolution monitoring. The premise upon which this approach is based is that the high-resolution features are predominately static and do not change significantly during the injection cycle of the storage process. We are developing strategies for seismic imaging though the approach is applicable to other imaging methods as well. The conventional seismic approach (Figure 38) that's used for hydrocarbon reservoirs is to produce a temporal sequence of high-resolution images or snapshots m_i , taken years apart as reservoir development progresses. Changes in the reservoir are detected by differencing the snapshots. For many reasons the differences often have much lower resolution than the individual snapshots, e.g., data acquisition is not repeatable and true reservoir changes are often larger scale. Our new approach (also Figure 4) is designed to build upon the high-resolution baseline image (produced as part of the site-selection process) with a sequence of low-resolution difference images Δm_i , each taken perhaps months or even weeks apart. To maximum acquisition repeatability, we propose to instrument the storage field with permanently emplaced seismic sources and detectors. To accelerate data processing and data analysis, the time-lapse data sets are recorded with reduced spatial and temporal sampling and coverage. The smaller data are then processed to explicitly parameterize a time-varying reservoir model (Day-Lewis *et al.*⁵⁸). Changes in fluid saturation (without the high-resolution static background) are directly imaged rather than through difference images. Moreover, we propose new survey geometries, acquisition schemes, and processing methods that are aimed at reducing costs and providing quasi-real-time monitoring capability. We are calling this new approach Adaptive Seismic Monitoring (ASM).

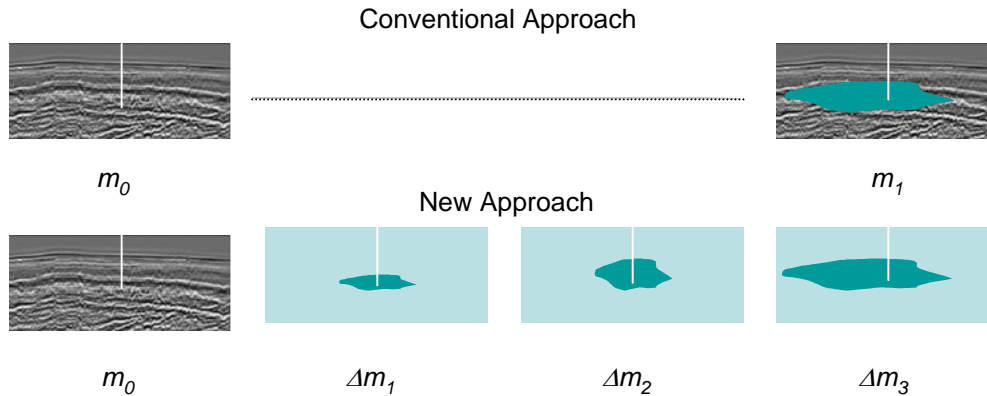


Figure 38: The conventional time-lapse imaging approach is to produce a sequence of snapshots, m_i , each taken perhaps years apart, e.g., m_0 and m_1 in the upper figure. Our new approach (ASM) is to produce a larger sequence of lower resolution difference images, Δm_i , taken perhaps months or even weeks apart. The baseline image m_0 is the same in both cases and comes from the site selection and characterization study.

An example of a new acquisition strategy is the Stanford Cross-Linear array illustrated in Figure 39. Seismic sources and detectors are distributed along three linear arrays, two along the surface and one along the injection borehole. The 3-axis arrays provide reduced 3-D resolution, but at greatly reduced acquisition and processing costs relative to the usual 2-D surface array. Both sources and receivers are permanently embedded to maximize survey repeatability and reduce deployment costs. Additional surface lines may be added or different sections of the Cross may be activated at different times to track the CO₂ front or to target specific reservoir zones or problems areas. Our new approach includes signal coding to permit the use of low-power sources for continuous operation; these attributes in particular enable quasi-real-time monitoring.

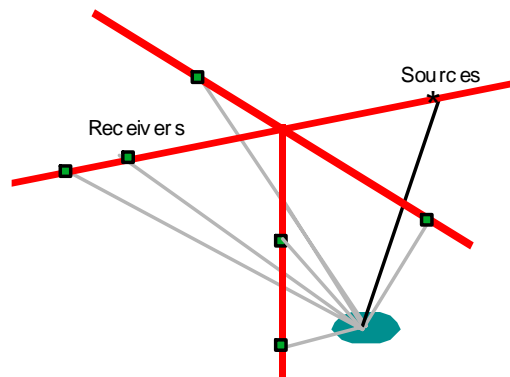


Figure 39: The Stanford Cross-Linear array incorporates 3-axis linear source/detector arrays emplaced along the surface and embedded along the injection borehole. Both in-plan and out-of-plane imaging is possible with this configuration. Sampling and the dimensions of the apertures of the arrays may be adjusted for resolution and subsurface coverage.

Results

A Synthetic Study on Seismic Monitoring

In order to test the many possibilities, we have developed some modeling tools for simulating the imaging of seismic data. So far, we are performing tests in two spatial dimensions. In this section, we present results for simulation study on full aperture imaging. During the next phase of the project, we will move to three spatial dimensions and limited aperture simulations. The synthetic model simulates shallow reservoir sands (e.g., less than 1000m) with a porosity of 35%. Four snapshots of the seismic velocity before and during CO₂ injection are shown in Figure 40. During injection, CO₂ replaces water in the formation resulting in assumed saturation levels of 20% CO₂ and 80% water. The P-wave velocity decreases from the pre-injection value of 2000 m/s to the post-inject value seen in the plumes of 1270 m/s. The changes in velocity are estimated using Gassmann's equation (Gassmann⁵⁶). Spatial dimensions, reservoir geometry, and seismic properties of the model are intended to be similar to those found at Sleipner.

We computed seismic datasets for each of the reservoir images shown in Figure 6. Each dataset was then processed using prestack depth migration (e.g., Bleistein & Gray⁵⁹) as the imaging method. The resulting time-lapse images of seismic reflectivity, shown in Figures 41, clearly show signatures of CO₂ saturation. Indeed the synthetic images show a skeletal resemblance to the time-lapse images from Sleipner, albeit with fewer details. We can see from Figure 41 that the amplitude differences in the time-lapse images indicate the changing contrast in reflectivity associated with changing CO₂ buildup just below impermeable horizontal interfaces. While there are also some imaging artifacts, the effects of the CO₂ are easily distinguished in these full aperture images. One of the imaging artifacts is the downward shift in the apparent depth of reflectors below CO₂ saturated zones. While an artifact of the image generation (wrong velocity), this downward shift may be used in a feature extraction scheme for real-time leak detection.

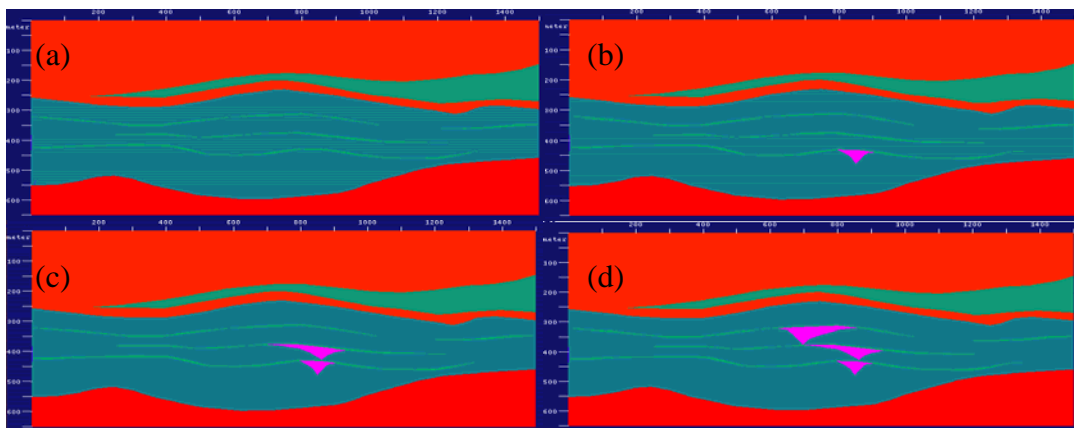


Figure 40: Four snapshots from a synthetic model of a reservoir experiencing CO₂ injection: (a) before injection; (b)-(d) three subsequent snapshots after injection illustrate the evolution of low velocity plumes of CO₂ generated as CO₂ migrates upward through shale breaks and accumulates below low permeability barriers.

3.

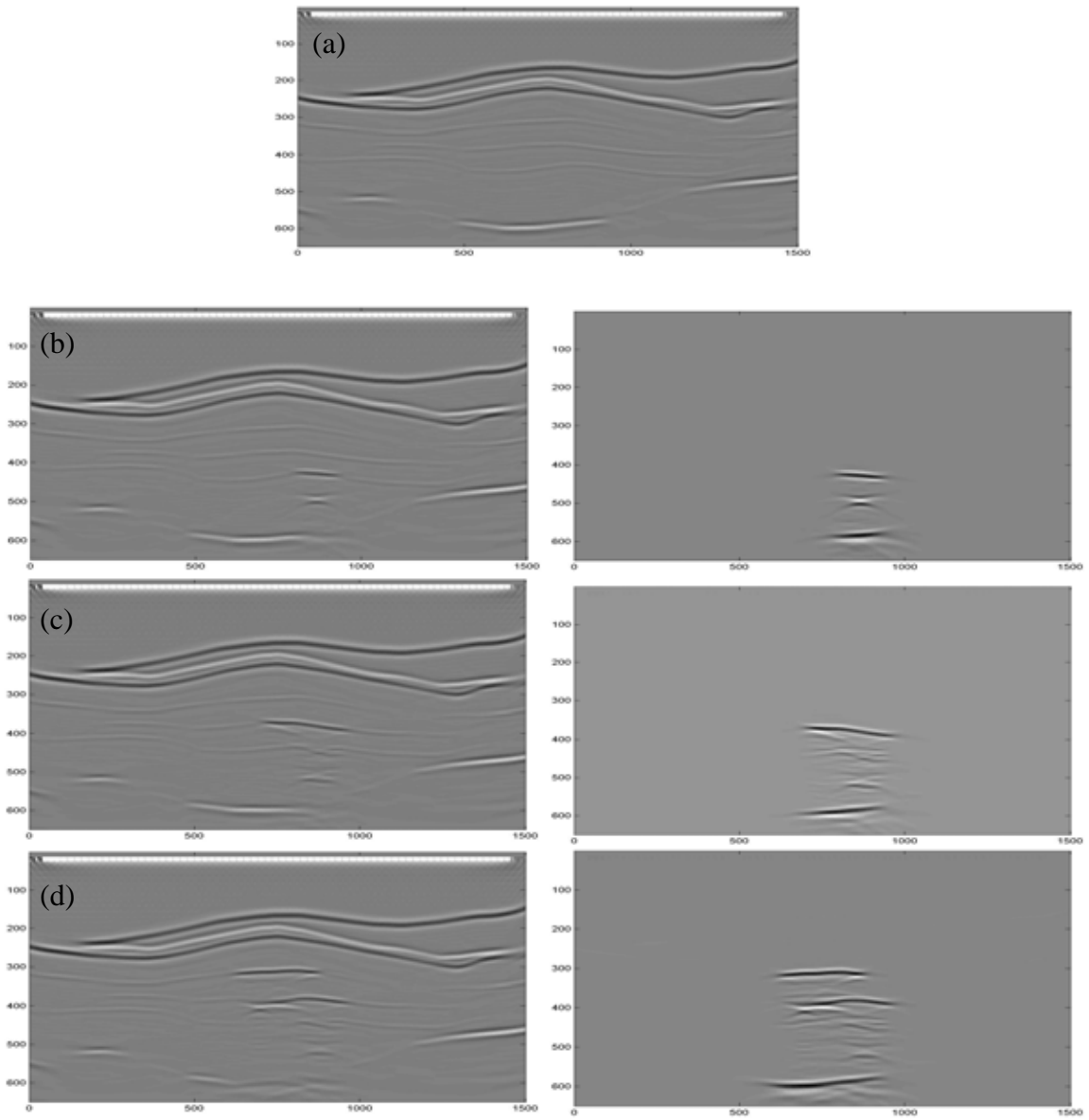


Figure 41: Time-lapse seismic images of the storage reservoir undergoing CO₂ injection. The images were created using prestack depth migration and full aperture datasets. (a) baseline; (b) – (d) time-lapse images (left column) and difference images (right column).

4.
5.
6.
7.

Diffraction Tomography

The simulations described above demonstrate that our modeling tools are fully capable of realistically capturing the effects of CO₂ seen in field data. Nevertheless, these realistic tools are much too complicated and slow to explore the parameter space required to develop Adaptive Seismic Monitoring. In order to study the important issues, we need a rapid way of investigating the effects of sampling, aperture dimensions, and signal frequency and bandwidth on image quality. To that end, we are using diffraction tomography based on the Born approximation as a solution to the Helmholtz equation (Devaney⁶⁰, Harris⁶¹, and Wu and Toksoz⁶²). While this method is elegant and especially useful for the simulation problem at hand, it has also been used on 2-D and 3-D field datasets (Bleistein and Gray⁶³, Kebo and Beydoun⁶⁴, Louie *et al.*⁶⁵). To differentiate the two imaging approaches presented here, diffraction tomography is best described as providing a quantitative velocity inversion based on weak inverse scattering theory while prestack depth migration is a qualitative “transpose” method based on back propagation. Diffraction tomography images the changes in velocity in the volume whereas migration images the changes in reflectivity at interfaces. Both have strengths and weaknesses. We needn't decide which to apply for the real-world monitoring problem at this time. While migration is far more practical for large field datasets, the analytical elegance of diffraction tomography is more useful for addressing the design problems of adaptive monitoring.

We assume that we have a baseline high-resolution seismic dataset prior to the injection of CO₂. The seismic wavefield used to produce the baseline image is denoted $U^o(\mathbf{r})$. When CO₂ is injected, the wavefield is perturbed to $U^1(\mathbf{r})$. The difference between the two is the scattered field $U^{sc}(\mathbf{r})$ that's generated by the injected CO₂. It can be shown that the scattered wavefield is linearly proportional to the Fourier spectrum of the changes in the medium created by the CO₂:

$$U^{sc}(\hat{\mathbf{r}}, \hat{\mathbf{s}}) = U^1 - U^o \approx \frac{U^o k^2}{4\pi r} e^{+ikr} \int_{\mathbf{v}} O(\mathbf{r}') e^{-ik_s \cdot \mathbf{r}'} d\mathbf{r}' = \frac{U^o k^2}{4\pi r} e^{+ikr} \tilde{O}(\mathbf{k}_s), \quad (22)$$

where $\tilde{O}(\mathbf{k}_s)$ is the Fourier transform of the perturbation in the medium $O(\mathbf{r})$ caused by the CO₂. The scattering vector $\mathbf{k}_s = (\hat{\mathbf{r}} - \hat{\mathbf{s}})\omega/c$ is used to define the set of angles and frequencies that can be used to sample the Fourier support of the medium with a combination of source and detector locations and signal frequencies. We use the spectral support as a filter to obtain a bandlimited spectrum of the medium. Inverse Fourier transform of the bandlimited spectrum gives a reconstruction of the medium for the considered geometry of sources and detectors and frequency bandwidth. Figure 42 shows the result of applying filters corresponding to surface seismic source-receiver apertures.

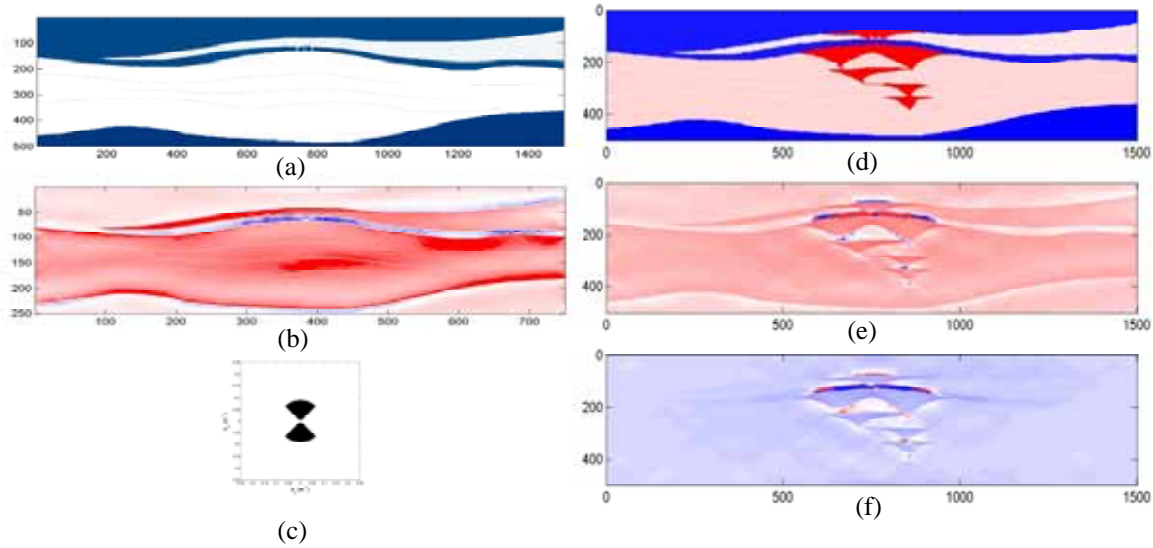


Figure 42: Time-lapse simulation from diffraction tomography: (a) Original earth model; (b) Diffraction tomogram for (a); (c) Spectral filter for a relatively wide surface seismic aperture; (d) Earth model with CO₂; (e) Diffraction tomogram of (d); (f) Difference tomogram. These images illustrate the ability of diffraction tomography to detect volumetric changes unlike migration that detects changes at the interfaces.

Barriers and Issues to large scale monitoring:

After years of injection, significant amounts of undissolved CO₂ could extend several kilometers laterally, potentially finding leakage pathways far away from the injection wellbore. These potential leak paths include abandoned boreholes and geological features such as faults and fractures in the subsurface. Monitoring must cover a significant portion of the reservoir if not the entire storage volume. Nevertheless, monitoring should not continue indefinitely nor should continuous monitoring be required during the entire life of the injection cycle. The questions of how much monitoring, how long and how often have not been answered and are expected to be responsive to regulatory and safety issues. Although monitoring costs may be relatively small in comparison with capture and transportation costs, they are nonetheless real expenses associated with disposal of a waste material. Efforts to improve the technical capability and reduce the direct cost of monitoring should be rewarded with easier public acceptance and truly safer reservoirs. It will be important to include monitoring as an integrated part of the site-specific sequestration project and begin the monitoring process with the baseline characterization study.

The ability to monitor a reservoir should be one of the many criteria considered when selecting a storage site. Also, the capability to predict the behavior or simulate the monitoring process is expected to be an important site-specific licensing issue. We have some concern regarding the conflicting requirements for leak detection and other safety issues (monitoring the entire storage volume) versus monitoring to assess process efficiency, i.e., following the front to track where the CO₂ is going. For this concern

alone, the monitoring strategy must be adaptive to meet changing resolution and coverage requirements with time. This is the guiding principle of our adaptive seismic-monitoring approach.

Progress

In the area of assessment of seal integrity, the projects are all beginning to take form. The biggest step we have made this year is developing important collaborations with a number of different companies, laboratories, and individuals. From these, we have gained resources, data and individual expertise and guidance that will aid in the success of our projects. Taken together, our three projects cover all of the possible options for geologic CO₂ sequestration. This will provide a meaningful breadth to our work. Individually, the projects will look deeply into the geomechanical issues unique to each specific setting. We are clearly moving towards a better understanding of how geomechanics influences the seal capacity, integrity and sequestration potential in the three geologic CO₂ storage options. This is a fundamental step in making widespread CO₂ sequestration operations a reality. Only through large-scale implementation will CO₂ sequestration make a significant impact in stabilizing atmospheric CO₂ concentrations.

In the area of flow prediction, we have completed a review of simulation tools available for CO₂ sequestration, and we now have working code available for compositional simulation of sequestration in gas fields, with or without condensate present. We also have a model working for streamline simulation of the injection period of aquifer sequestration with dissolution of CO₂ in the brine and gravity segregation. We are engaged presently in work to understand the interplay of physical mechanisms that act on various time scales for aquifers and coalbeds. Those analyses will guide the selection of simulation methods and tools that will be the toolkit for designers of sequestration projects. In some areas, continued development of the streamline approach will be useful, but for others, other simulation tools will be required. The overall objective is to provide tools for flow prediction that represent accurately the physical mechanism that dominate flow and storage and that are efficient enough that they can be used to design the hundreds of projects at the scale that will be required for widespread application of geologic sequestration.

In the monitoring area, we have completed a scoping study that considered a wide variety on subsurface monitoring methods. From this study, we concluded that seismic is the generic preference for the widest range of storage scenarios, container depths, and geological environments. We next turned our attention to the development of cost-effective seismic-monitoring strategies that could be adapted to changing reservoir conditions. We developed simulation capability involving rock and coal properties with CO₂, seismic modeling, and imaging. Our simulation of a simplified model for Sleipner is remarkably similar to the Sleipner field observations. Moreover, we have developed a simulation tool, in diffraction tomography, for rapidly investigating the tradeoffs among imaging issues such as data-acquisition geometry, sampling, signal frequency and signal bandwidth. This rapid simulation capability has been tested but has not yet been used to design or optimize the Adaptive Seismic Monitoring system. This will come in the next phase of the project. Other activities not described in detail above include specific

considerations for monitoring enhanced coal bed methane production (Akintunde, 2004) and the estimation of seismic-attenuation properties for rocks at low seismic frequencies.

Future Plans

In the seal integrity portion of the project in the next months, through the continued collaboration with Dr. Rutqvist, we expect to develop the simulations of CO₂ sequestration for the specific setting like the one we are trying to model in the Powder River Basin. We continue to work on the Ohio River Valley Storage Project, with Amie Lucier working on the project with collaborators at the Schlumberger-Doll Research Laboratory through May. Our geomechanical model and fracture characterization will be complete by mid-summer. Amie Lucier will also work on developing a geomechanical workflow for assessing reservoir suitability using South Eugene Island 330 as a case study during a fall internship at the ExxonMobil Exploration Company.

Work in the area of flow prediction will proceed on several fronts. We will use streamline simulations of aquifer injection to create a suite of initial conditions for a set of high-resolution, high-order finite difference simulations to examine the interplay of heterogeneity, dissolution, gravity segregation of injected CO₂, slow density-driven convection in the brine phase, and diffusion. Those simulations will allow us to judge which simulation tools are appropriate for prediction of what happens in an aquifer after injection has ceased based on the physics of the displacements. We will also continue to develop the physical picture and related simulation tools for coalbeds, and we will continue to investigate experimentally the behavior of multicomponent adsorption of mixed gases in coal.

Future work on monitoring falls into two areas:

- (1) Development of specific technology for the assessment and implementation of an adaptive monitoring system. This will include data acquisition, data processing, and analysis and leak-detection procedures. Although we're focusing our attention on seismic, the lessons learned and procedures developed will apply to other methods (deformation, electromagnetic,...) as well. This effort involves considerable numerical simulation studies, using both the realistic migration toolkit as well as the diffraction tomography toolkit. We anticipate testing our strategies for an adaptive seismic-monitoring system on field data. The final piece of the monitoring strategy we plan to pursue is the analysis and interpretation tools for container assessment and leak detection.
- (2) Development of a decision procedure and scoring system for assessing the suitability of a site for monitoring. This process of decision analysis will be similar to the reservoir analysis used to estimate the likelihood of success of 4-D seismic projects in the petroleum industry. It will include site-specific information such as reservoir depth, fluid history, pressure history, rock type, overburden rock, seismic data quality, etc. Of course, however, our scoring system will be based of CO₂ storage issues rather than oil and gas recovery issues.

Publications

Papers, reports, and theses

1. Cakici, M.D., Cooptimization of Oil Recovery and Carbon Dioxide Storage, Engineer Thesis, Stanford University, December 2003.
2. Seto, C.J., Compositional Streamline Simulation: An Application to Gas Injection for Enhanced Condensate Recovery in Condensate Reservoirs, MS Report, Stanford University, June 2003.
3. Wynn, D., Survey of Geophysical Monitoring Methods for Monitoring CO₂ Sequestration in Aquifers, M.S. Thesis, Department of Geophysics, Stanford University, 2003.
4. Orr, F.M., Jr., Storage of Carbon Dioxide in Geologic Formations, invited paper for Distinguished Author Series, *J. Petroleum Technology*, in review, April, 2004.

Presentations

1. Orr, F.M., Jr.: "Energy and Global Change: CO₂ Sequestration in the Earth's Crust and Deep Ocean," Petroleum Engineering Department, University of Texas at Austin, March 31, 2003.
2. Orr, F.M., Jr.: "CO₂ Sequestration in the Earth's Crust and Deep Ocean," National Research Council Committee on Alternative Strategies for Future Production and Use of Hydrogen, April 23, 2003.
3. Seto, C.J., Jessen, K., and Orr, F.M., Jr.: "Enhanced Condensate Recovery and CO₂ Sequestration," IEA Workshop on Enhanced Oil Recovery, Regina, September 7-10, 2003.
4. Orr, F.M., Jr., Zoback, M.D., and Kavscek, A.R.: "Geologic Sequestration of CO₂: Storage Mechanisms and Potential for Leaks," MIT Carbon Sequestration Forum, Cambridge, November 6, 2003.
5. Orr, F.M., Jr.: "Energy and Global Change: CO₂ Sequestration in the Earth's Crust and Deep Ocean," Chemical Engineering Department, University of Utah, November 18, 2003.
6. Colmenares, L. and Zoback, M. D., CO₂ Sequestration and ECBM in the Powder River Basin: *Eos. Trans. AGU*, 84(46), Fall Meet. Suppl., Abstract GC32A-02, 2003.
7. Orr, F.M., Jr.: "Energy and Global Change: CO₂ Sequestration in the Earth's Crust and Deep Ocean," Society of Petroleum Engineers, Los Angeles Section, December 9, 2003.
8. Akintunde, O.M., Harris, J.M., Mukerji, T. and Urban, J., A Feasibility Study for CO₂ Monitoring in Coal Bed Methane (CBM), A paper presented at the American Association of Petroleum Geologists (AAPG) Annual Convention, Dallas, U.S.A, 2004.
9. Orr, F.M., Jr.: "CO₂ Sequestration in the Earth's Crust and Deep Ocean," Guest lecture, Mechanical Engineering 370, Stanford University, April 8, 2004.
10. Lucier, A. and Zoback, M. D., CO₂ Sequestration in Depleted Oil and Gas Reservoirs: A Proposed Workflow for Assessing Reservoir Suitability in the Gulf of Mexico, Case Study Applied to South Eugene Island 330: Proceedings from 3rd Annual Conference on CO₂ Sequestration, Alexandria, VA, May 3-6, 2004.

References

1. Jessen, K., and Orr, F.M., Jr., Gas Cycling and the Development of Miscibility in Condensate Reservoirs: SPE 84070, presented at the SPE Annual Technical Conference, Denver, October 5-8, 2003.
2. Peng, D.Y. and Robinson, D.B., A New Two-Constant Equation of State, *Ind. Eng. Chem. Fund* 15, 59-64, 1976.
3. Jhaveri, B.S., and Youngren, G.K., Three-Parameter Modification of the Peng-Robinson Equation of State to Improve Volumetric Predictions, *Soc. Pet. Eng. Res. Eng.*, 1033-1040, 1988.
4. Ennis-King, J., and Paterson, L., Role of Convective Mixing in the Long-Term Storage of Carbon Dioxide in Deep Saline Formations, SPE 84344, presented at the SPE Annual Technical Conference, Denver, October 5-8, 2003.
5. Kumar, A., et al., Reservoir Simulation of CO₂ Storage in Deep Saline Aquifers, SPE 89343, presented at the SPE/DOE 14th Symposium on Improved Oil Recovery, Tulsa, April 17-21, 2004.
6. Johnson, J.W., and Nitao, J.J., Reactive Transport Modeling of Geologic CO₂ Sequestration at Sleipner, in *Greenhouse Gas Control Technologies* Vol. I, J. Gale and Y. Kay, Eds., Elsevier, 327-332, 2003.
7. Ohga, K., et al., Fundamental Tests on Carbon Dioxide Sequestration into Coal Seams, in *Greenhouse Gas Control Technologies* Vol. I, J. Gale and Y. Kay, Eds., Elsevier, 531-537, 2003.

8. Zhu, J. *et al.*, Analytical Theory of Coalbed Methane Recovery by Gas Injection, *Soc. Pet Eng. J.*, 371–379, December, 2003.
9. Parson, E.A., and Keith, D.W., Fossil Fuels Without CO₂ Emissions, *Science* 282, 1053-1054, 1998.
10. Gale, J., Geological Storage of CO₂: What's Known, Where Are the Gaps, and What More Needs to Be Done, in *Greenhouse Gas Control Technologies*, Vol. I, J. Gale and Y. Kaya, Eds., Elsevier, 207-212, 2003.
11. *World Energy Outlook 2002*, International Energy Agency, Paris, p. 30, 2002.
12. Torp, T.A., and Gale, J., Demonstrating Storage of CO₂ in Geological Reservoirs: The Sleipner and SACS Projects, in *Greenhouse Gas Control Technologies* Vol. I, J. Gale and Y. Kay, Eds., Elsevier, 311-316, 2003.
13. Finkbeiner, T., *et al.*, Stress, Pore Pressure and Dynamically-Constrained Hydrocarbon Column Heights in the South Eugene Island 330 field, Gulf of Mexico, *Amer. Assoc. Petrol. Geol. Bull.*, 85, 1007-1031, June 2001.
14. Jimenez, J.A., and Chalaturnyk, R.J., Integrity of Bounding Seals for Geologic Storage of Greenhouse Gases, SPE/IRSM 78196, presented at the SPE/IRSM Rock Mechanics Conference, Irving, Oct. 20-23, 2002.
15. Arts, R., *et al.*, Monitoring of CO₂ Injected at Sleipner Using Time Lapse Seismic Data, in *Greenhouse Gas Control Technologies* Vol. I, J. Gale and Y. Kaya, Eds., Elsevier, 347-352, 2003.
16. Hoversten, G.M., *et al.*, Crosswell Seismic and Electromagnetic Monitoring of CO₂ Sequestration, in *Greenhouse Gas Control Technologies* Vol. I, J. Gale and Y. Kaya, Eds., Elsevier, 371-376, 2003.
17. Wilson, E.J., and Keith, D.W., Geologic Carbon Storage: Understanding the Rules of the Underground, in *Greenhouse Gas Control Technologies* Vol. I, J. Gale and Y. Kaya, Eds., Elsevier, 229-234, 2003.
18. Reeves, S., Assessment of CO₂ Sequestration and ECBM Potential of U.S. Coalbeds, DOE Topical Report, February 2003.
19. Gupta, N., The Ohio River Valley CO₂ Storage Project: Project Overview for Carbon Sequestration Program Review 2003, Battelle, May 12, 2003.
20. Pennwell MAPSearch, Gulf of Mexico Pipeline Systems Map, Pennwell Publishing Company, 2000.
21. Pruess, K., Oldenburg, C., and Moridis, G., TOUGH2 User's Guide, Version 2.0, Technical Report LBNL – 43134, Lawrence Berkeley National Laboratory, 1999.
22. Webb, S., Modification of TOUGH2 for Enhanced Coal Bed Methane Simulations, Technical Report SAND2003-0154, Sandia National Laboratory, 2003.
23. Finkbeiner, T., Zoback, M.D., Flemings, P.B., and Stump, B.B., Stress, pore pressure, and dynamically constrained hydrocarbon columns in the South Eugene Island 330 field, northern Gulf of Mexico, *AAPG Bulletin*, 85(6), 1007-1031, 2001.
24. Alexander, L.L., Flemings, P.B., Geologic Evolution of a Pliocene-Pleistocene Salt-Withdrawal Minibasin: Eugene Island Block 330, Offshore Louisiana, *AAPG Bulletin*, 79(12), 1737-1756, 1995.
25. Alexander, L.L., and Handschy, J.W., Fluid flow in a faulted reservoir system: Fault trap analysis for the Block 330 Field in Eugene Island, South Addition, offshore Louisiana, *AAPG Bulletin*, 82(3), 387-411, 1998.
26. Gordon, D.S., Flemings, P.B., Generation of overpressure and compaction-driven fluid flow in a Plio-Pleistocene growth-faulted basin, Eugene Island 330, offshore Louisiana, *Basin Research*, 10, 177-196, 1998.
27. Losh, S., Eglinton, L., Schoell, M., Wood, J., Vertical and lateral fluid flow related to a large growth fault, South Eugene Island Block 330 Field, offshore Louisiana, *AAPG Bulletin*, 83(2), 244-276, 1999.
28. Stump, B.B., Flemings, P.B., Overpressure and fluid flow in dipping structures of the offshore Gulf of Mexico (E.I. 330 field), *Journal of Geochemical Exploration*, v. 69-70, p. 23-28, 2000.
29. Losh, S., Walter, L., Meulbroek, P., Martini, A., Cathles, L., and Whelan, J., Reservoir fluids and their migration into the South Eugene Island Block 330 reservoirs, offshore Louisiana, *AAPG Bulletin*, 86(8), 1463-1488, 2002.
30. Nitao, J.J., Reference Manual for the NUFT flow transport code, Version 2.0. Lawrence Livermore National Laboratory, 1998.
31. Johnson, J.W., Oelkers, E.H., and Helgeson, O.H., SUPCRT92: A software package for calculating the standard molal thermodynamic properties of minerals, gases, aqueous species, and reactions from 1 to 5000 bars and 0 to 1000 C, *Computers and Geosciences* 7, 899-947, 1992.

Project Results: Geologic CO₂ Sequestration

32. Lichtner, P.C, FLOTRAN user's manual: two-phase nonisothermal coupled thermal-hydrologic-chemical (THC) reactive flow & transport code, Technical Report LA-UR-01-2349, Los Alamos National Laboratory, 2003.
33. White, M.D., and Oostrom, M., STOMP Subsurface Transport Over Multiple Phases: Users's Guide, Version 2.0. Technical Report PNNL-14286, Pacific Northwest National Laboratory, 2003.
34. Chang, Y.B., Development and Application of an Equation of State Compositional Simulator, PhD Dissertation, University of Texas at Austin, 1990.
35. Sams, W. N., Bromhal, G., Odusote, O., Jikich, S., Ertekin, T., and Smith, D. H., Simulating Carbon Dioxide Sequestration/ECBM Production in Coal Seams: Effects of Coal Properties and Operational Parameters, SPE 78691, presented at the 2002 SPE Eastern Regional Meeting. Lexington, KY, 23-25 October 2002.
36. Seidle, J. P., and Arri, L. E., Use of Conventional Reservoir Models for Coalbed Methane Simulation, paper CIM/SPE 90-118, presented at The Canadian Institute of Mining/Society of Petroleum Engineers International Technical Meeting, Calgary, AB., June 10-13, 1990.
37. Van de Meer, B., An Excellent Simulation Tool: SIMED II, *Information*. TNO-NITG, 12-14, May 2004.
38. *GEM 2003.10 User's Guide*, CMG Computer Modelling Group, Calgary, AB., 2003.
39. Shi, J.-Q., and Durucan, S., Gas Storage and Flow in Coalbed Reservoirs: Implementation of a Bidisperse Pore Model for Gas Diffusion in Coal Matrix, SPE84342 presented at the SPE Annual Technical Conference, Denver, CO, October 5-8, 2003.
40. Shi, J.-Q., and Durucan, S., A bidisperse pore diffusion model for methane displacement desorption in coal by CO₂ injection, *Fuel* 82, 1219-1229, 2003.
41. Reeves, S. and Pekot, L., Advanced Reservoir Modeling in Desorption-Controlled Reservoirs, SPE 71090, presented at the SPE Rocky Mountain Petroleum Technology Conference, Keystone, CO, May 21-23, 2001.
42. *Eclipse Technical Manual: The Coal Bed Methane Model*, Schlumberger, 2003.
43. Seto, C.J., Compositional Streamline Simulation: An Application to Gas Injection for Enhanced Condensate Recovery in Condensate Reservoirs, MS Report, Stanford University, June 2003.
44. Cakici, M. D., Cooptimization of Oil Recovery and Carbon Dioxide Storage, Engineer Thesis, Stanford University, December 2003.
45. Johnson, J.W., Knauss, K.G., Nitao, J.J., and Steefel, C.I., Reactive transport modeling of geologic CO₂ sequestration in saline aquifers: the influence of intra-aquifer shales and the relative effectiveness of structural solubility and mineral trapping during prograde and retrograde sequestration, presented at the First National Conference on Carbon Sequestration, May 2001.
46. Amyx, J.W., Bass, D.M. Jr., and Whiting, R. L., *Petroleum Reservoir Engineering-Physical Properties*, McGraw-Hill, New York, 1960.
47. McHardy, J., and Sawan, S.P., *Supercritical Fluid Cleaning: Fundamentals, Technology, and Applications*, Noyes Publications, Westwood, NJ, 1998.
48. Zhou, D., Fayers, F.J., and Orr, F.M., Jr., Scaling of Multiphase Flow in Simple Heterogeneous Porous Media, Proc., Fourth Symp. on Multiphase Transport in Porous Media, New Orleans, Nov. 28-Dec. 3, 1993.
49. Yan, W., Michelsen, M.L., Stenby, E.H., Berenblyum, R.A., and Shapiro, A., Three-phase Compositional Streamline Simulation and Its Application to WAG, SPE 89440, Tulsa, 2004.
50. Close, J.C., Natural Fractures in Coal: Chapter 5, *AAPG Special Publication*, 119-132, 1993.
51. Gamson, P.D., Beamish, B.B., and Johnson, D.P., Coal Microstructure and Micropermeability and Their Effect on Natural Gas Recovery, *AAPG Bulletin*, 1102, 1992.
52. Grogan, A.T., Pinczewski, V.W., Ruskauff, G.J. and Orr, F.M., Jr., Diffusion of Carbon Dioxide at Reservoir Conditions: Models and Measurements, *Soc. Pet. Eng. Res. Eng.*, 3(1), 93-102, 1988.
53. Mazunder, S., Plug, W.-J., and Bruning, H., Capillary Pressure and Wettability Behaviour of Coal-Water-Carbon dioxide System, SPE 84339, presented at the SPE Annual Technical Conference and Exhibition. Denver, October 5-8, 2003.
54. Wynn, D., Survey of Geophysical Monitoring Methods for Monitoring CO₂ Sequestration in Aquifers, M.S. Thesis, Department of Geophysics, Stanford University, 2003.
55. Wang, Z and Nur, A., Effect of CO₂ flooding on wave velocities in rocks with hydrocarbons, *Soc. Petr. Eng. Res. Eng.*, 3, 429-439, 1989.

56. Gassmann, F., Elastic Waves through a Packing of Sphere, *Geophysics*, 16, 673-685, 1951.
57. Yu, G., Vozoff, K. and Durney, D.U., The Influence of Confining Pressure and Water Saturation on Dynamic Elastic Properties of Some Permian Coals, *Geophysics* 58, 30-38, 1993.
58. Day-Lewis, F., Harris, J.M., and Gorelick, S., Time-lapse Inversion of Crosswell Radar Data, *Geophysics*, 67(6), 1740-1752, November-December 2002.
59. Bleistein, N., and Gray, S.H., From the Hagedoorn Imaging Technique to Kirchhoff Migration and Inversion, *Geophys. Prosp.* 49(6), 2001.
60. Devaney, A.J., Geophysical Diffraction Tomography, *IEEE Trans. Geosci. Remote Sensing*, GE-22, 3-13, 1984.
61. Harris, J.M., Diffraction Tomography with Arrays of Discrete Sources and Receivers, *IEEE Trans. Geosci. Remote Sensing*, GE-25, 448-455, 1987.
62. Wu, R.S., and Toksoz, M.N., Diffraction tomography and multisource holography applied to seismic imaging, *Geophysics*, 52(1), 1987.
63. Bleistein, N., and Gray, S.H., An Extension of the Born Inversion Procedure to Depth Dependent Velocity Profiles, *Geophys. Prosp.*, 33, 999-1022, 1985.
64. Keho, T.H., and Beydoun, W.B., Paraxial Ray Kirchhoff Migration, *Geophysics* 53, 1540-1546, 1988.
65. Louie, J.N., Clayton, R.W., and LeBras, R.J., Three-dimensional imaging of steeply dipping structure near the San Andreas fault, Parkfield, California, *Geophysics*, 53, 176-185, 1988.

Contacts

M. Akintunde: olusoga@pangea.stanford.edu
L. Colmenares: lbcf@pangea.stanford.edu
J. M. Harris: harris@pangea.stanford.edu
M. Hesse: mhesse@pangea.stanford.edu
K. Jessen: krisj@pangea.stanford.edu
A. R. Kovscek: kovscek@pangea.stanford.edu
A. Lucier: luciera@pangea.stanford.edu
T. Mukerji: mukerji@pangea.stanford.edu
F. M. Orr Jr.: fmorr@pangea.stanford.edu
Y. Quan: quany@pangea.stanford.edu
C. J. Seto: cjseto@pangea.stanford.edu
C. Xu: xct7015@pangea.stanford.edu
G. Q. Tang: gtang@pangea.stanford.edu
M. D. Zoback: zoback@pangea.stanford.edu